What Einstein left out:
Gaining clarity in modern physics curricula

William G. Harter

University of Arkansas, Department of Physics, Fayetteville AR 72701

(Dated: November 14, 2017)

Abstract

It is not widely known that crossed laser waves or waveguides produce a Minkowski space-time coordinate system. Less known is that geometry exposed by such a system can add clarity to the derivation and development of special relativity and quantum mechanics. Such a combination of these two pillars of modern physics serves to demystify both in ways that are not available if either stands alone. When explained in concert, students get clearer and more powerful theory and more convenient computational tools.

(At current date above, this is undergoing final review and editing)

CONTENTS

References

[1] Lewis Carroll. Epstein. *Relativity visualized*. Insight Press, San Francisco, 1985. ISBN 093521805X 9780935218053. [Cited on page 24.]

[2] Albert Einstein. Über einen die Erzeugung und Verwandlung des Lichtes betreffenden heuristischen Gesichtspunkt. (German) [On the production and transformation of light from a heuristic viewpoint]. 322(6):132–148, 1905. ISSN 0003-3804. doi:http://dx.doi.org/10.1002/andp.19053220607. URL http://www.zbp.univie.ac.at/einstein/einstein1.pdf. [Cited on page 36.]

[3] Louis de Broglie. Waves and quanta. *Nature*, 112:540, October 1923. [Cited on page 36.]

[4] Max Planck. Zur theorie des gesetzes der energieverteilung im normalspectrum. *Deutsche Physikalische Gesellschaft*, 2(237–245), 1900. [Cited on page 36.]

[5] Wikipedia. Phlogiston theory — wikipedia, the free encyclopedia, 2017. URL https://en.wikipedia.org/w/index.php?title=Phlogiston_theory&oldid=793410106. [Online; accessed 10-August-2017]. [Cited on page 37.]

[6] Niels Bohr. Der bau der atome und die physikalischen und chemischen eigenschaften der elemente. *Z. Physik*, 9(1):1–67, 1922. doi:10.1007/BF01326955. URL http://dx.doi.org/10.1007/BF01326955. [Cited on page 38.]

[7] E Schrödinger. Schrodinger's protests about prevailing quantum mechanical interpretations are widely circulated, 1910–1961. See smart groups in Schrodinger-Erwin_Works.bib. [Cited on page 38.]

[8] K.W. Ford. *Building the H Bomb: A Personal History*. World Scientific Publishing Company Pte Limited, 2015. ISBN 9789814632072. URL https://books.google.com/books?id=1bHToQEACAAJ. [Cited on page 42.]

[9] R.P. Feynman and C. Sykes. *No Ordinary Genius: The Illustrated Richard Feynman*. Norton, 1994. ISBN 9780393313932. URL https://books.google.com/books?id=1HxzLaPYo2IC. [Cited on page 47.]

[10] P. A. M. Dirac. Forms of relativistic dynamics. *Reviews of Modern Physics*, 21:392–399, Jul 1949. [Cited on page 47.]

[11] L.M. Brown. *"Feynman's Thesis" A New Approach to Quantum Theory*. WS, World Scientific, 2005. ISBN 9789814480147. URL https://books.google.com/books?id=z93ICgAAQBAJ. An

edited copy of 1941 thesis and discussion of RPF Space-time approach to non-relativistic quantum mechanics, Rev. Mod. Phys. 20 (1948) pp. 367-387; and R. P. Feynman and A. R. Hibbs, Quantum Mechanics and Path Integrals (McGraw-Hill 1965). [Cited on page 47.]

[12] Albert Einstein, 1942. URL https://sec2.einstein.caltech.edu/archives/scans/015/15294.pdf. I shall never believe that god plays dice with the universe - Albert Einstein Archives, The Jewish National University Library, The Hebrew University of Jerusalem (www.albert-einstein.org), Letter to Cornelius Lanczos, March 21, 1942. [Cited on page 54.]

I. INTRODUCTION

From about 1918 forward, Albert Einstein became a name associated with genius and discovery of modern physics particularly with regard to relativity and quantum theory. These new ideas seemed so startling and beyond previous thought. Many doubted that more than a handful of scientists could begin to comprehend them. Even now in the 21^{st} century we find students reactions to courses in special relativity (SR) and quantum mechanics (QM) contain comments such as (paraphrasing) *"Well I didn't understand all of that but I don't think the instructor did either!"*

One may ask if all that is mysterious or difficult about SR and QM must exist forever. More to the point, should the original logic used to discover a new area be its exclusive pedagogy henceforward? Surely a clarifying change of view point should be welcome to students of all ages. The Einstein library project provides suggestive paths to search for clarity. First it reminds us that in spite of great brilliance there is no doubt that Albert Einstein was human and to err is to be human. Evidence of that in both his personal and scientific life can help to guide those who follow. A particular mishap involves Einstein's interaction with Herman Minkowski, his mathematical physics professor, who scolded him for being a "lazy dog". Shortly after Einstein's *annus mirabilis* of 1905, Minkowski wrote to Einstein about graphs he had discovered to help unravel subtleties of SR. Einstein did not answer. Minkowski published in 1908 but then died in 1909. It is tragic that SR texts do not fully employ his wonderful geometric aid. The thrust of this article is to rectify this slight using optical wave grids of Minkowski coordinates that leads to a powerful geometric and algebraic derivation of fundamentals for both SR and QM wherein they merge into a single subject. Neither has to stand alone in future curricula, indeed, *they should not.* Wave interference is our most precise tool to measure relative distance, time, and velocity. So this new merged subject is named *relawavity* (RW).

This article first exposes how plane wave interference in crossed laser beams, a laser cavity, or Fabry-Perot interferometer makes a Minkowski spacetime lattice out of wave nodes. RW geometry of this lattice fixes seven oversights inherent to a standard SR approach and leads to a QM theory derivation.

(1) RW deals with 1^{st}-order effects *first*, in particular, Doppler shifts. Most treatments of SR jump to quite tiny and mysterious 2^{nd}-order effects (Lorentz contraction or Einstein

time-dilation). The relawavity approach makes it easy to see the latter are just due to the former and not so mysterious.

(2) RW uses a *(υ,cκ)*-dispersion-plot of frequency vs wavenumber. It is an oversight by both Einstein and Minkowski particularly since reciprocal space-time lattice geometry matches that of Minkowski's *(x,ct)* lattice. Students appreciate the idea of a wave-keyboard or Fourier control-panel for simplifying *(x,ct)* wave dynamics.

(3) RW deals with the showstopper axiom of constant light speed c. Critical-thinking students deserve a way to "see c"and clarify what we call Evenson's RW Axiom: *All colors go c.* (After Fig.2)

(4) RW shows quickly how Galileo's failed velocity addition is replaced by addition of parameter ρ_{RS} (called *rapidity*), the natural log of Doppler shift ratio (R/S)= $\upsilon_{RECEIVER}/\upsilon_{SOURCE}$. (After Fig.3)

(5) RW provides a context for the space-proper-time approach to SR that uses the *stellar aberration angle* σ as a 1^{st}-order parameter. (Also known as a waveguide **k**-angle.) (After Figs.9 - 12)

(6) RW geometry uses phase and group wave properties to map space-time and per-space-time geometry by each phase and group wave's period, wavelength, frequency, and wavenumber dependency on parameters ρ, σ, and β. (β=u/c is the relativity parameter in Standard SR.) (Table I. displays this all.)

(7) RW wave $(\upsilon,c\kappa)$-dependencies then derive quantum relations of Planck (1900), De-Broglie (1921), Compton and basic QM theory while giving insights into classical or semiclassical mechanics. This lets a student understand more deeply what is behind quantities such as energy, momentum, Hamiltonian, Lagrangian, action, and mass and lets us distinguish three kinds of mass. (Figs.18-22)

It is remarkable that so much physics arises from relatively simple steps of geometric logic based upon a single axiom, namely Evenson's *All colors go c*, that virtually proves itself. (Derivation following Fig.1 and Fig.2 uses linear Doppler effects.) Here laser technology, unknown until after 1960, now sheds light on SR and QM theory.

Minkowski's plot geometry starts with *Relativity Baseball Diamonds* (RBD) in Figs.1, 4, and 5 that provide a top-down physics-first approach. Thales (600 *BCE*) geometric means then build upon the RBD to derive the circular-hyperbolic *Trigonometric Road Maps* (TRM) in Fig.7.

Most instructors are unaware that TRM dual circular-hyperbolic functions involve a sextet of circular functions of σ co-equal to a sextet of hyperbolic functions of ρ : $\sin\rho = \tanh\rho$, $\tan\rho = \sinh\rho$, $\cos\sigma = \mathrm{sech}\rho$, $\sec\sigma = \cosh\rho$, and $\csc\sigma = \coth\rho$, $\cot\sigma = \mathrm{csch}\rho$. Each of the six pairs define one or more of six SR functions in space-time (x-contraction, t-slowing, *etc.*) and one or more of six QM functions in per-space-time (momentum-p, Lagrangian-L, etc.). An alternative way to do SR uses the σ-sextet.

TRM serve as templates to diagram laser guide modes, Lagrangian or Hamiltonian functions, and transition properties such as Compton recoil effects and scattering geometry shown by Feynman diagrams in either (x,ct) or (υ,cκ). Web-Based TRM and RGB provide adjustable or animated plots of varying complexity, a welcome facility for a student who has completed some hand-drawn examples by ruler & compass. However, one should not minimize the pedagogical values of tactile exercises.

This first relawavity presentation is simplified by leaving out an important part of quantum mechanics, namely optical polarization and spin mechanics. Such an omission is shared by the early creators of quantum theory until Jordan, Pauli, Dirac, and others developed spinor theories for electron spin and orbital mechanics. It should be noted that John Stokes described a spin vector for light waves in 1863 and in 1843 Hamilton developed quaternion algebra later related to that of spinors. So electromagnetic waves used in the following development are restricted to one plane of polarization with field **E** normal to beam **k**-direction of propagation. This restricts the waveguide modes to the simplest TE (Transverse-Electric) type. Including full U(2)×U(2) polarization for each wave is a work in progress for a longer and more complex article.

II. MAPPING SPACE AND TIME USING LIGHTWAVES

Relawavity begins by describing interference of a pair of CW (Continuous Wave) laser beams of frequency υ=600THz=600·10^{12}Hz=6·10^{14}sec^{-1} shown colliding head-on in Fig.1a-c. As is now common in the *gedanken*-experiments of the modern quantum optics literature, we imagine points of interest *A, B,* and *C* manned or woman-ed by real people Alice, Bob, and Carla. Alice and Carla aim their beams at Bob who sees their waves add up to a standing-wave space-time interference pattern as beams collide in Fig.1b.

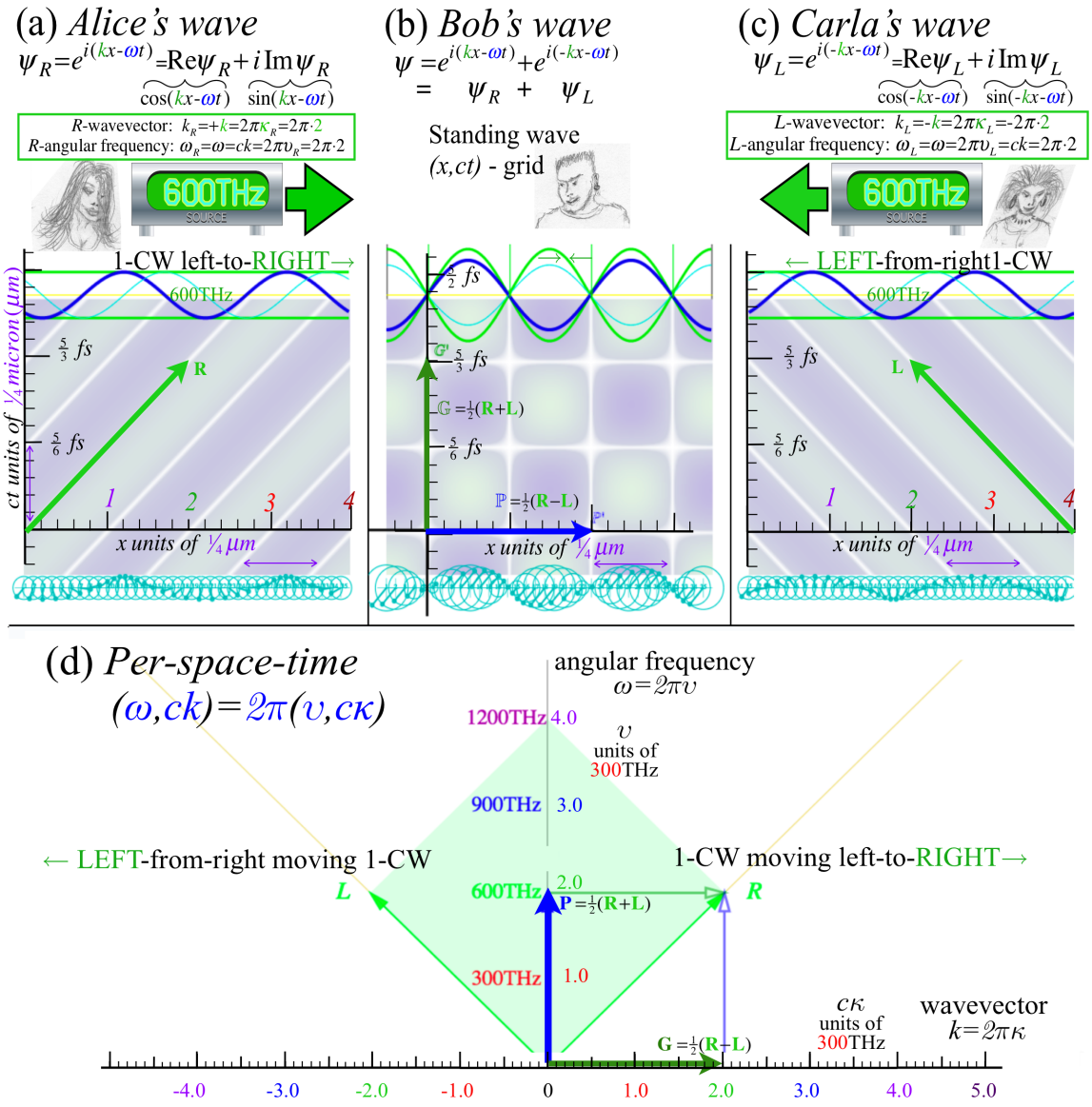

FIG. 1: (x,ct)-plot for (a) Alice Ψ_R, (b) Bob $\Psi_R+\Psi_L$, (c) Carla Ψ_L (d) $(c\kappa,\upsilon)$-plot of (b)

Light or dark regions in Fig.1a-c are, respectively, crests or troughs of real part (ReΨ) tracing a dark blue cos-curve that lags behind a cyan (ImΨ) sin-curve by 90°-phase. Phasor circles (ReΨ,ImΨ) below Fig.1a-c serve as clocks with ReΨ axis up and ImΨ axis left. (Ideally, electric field amplitudes **E** ReΨ should be normal to *(x,ct)*-plane.) Here, the focus is on real-zero (ReΨ=0) loci (the white lines in Fig.1a-c). In Fig.1b they form Cartesian space-time coordinate grids and in Fig.4, Minkowski grids. First, wave variables of space-

time and their inverse units are reviewed. (These often go missing in US curricula.)

A. Space-time grid units

Each of the upper three plots (Fig.1a-c) has vertical axis-ct time span of $c\Delta t$=10/3 *fs* (1 *femto-sec.*=10^{-15} *s.*) and horizontal x-axis span of Δx=1μm (1*micron* =10^{-6}*meter*). Two 600THz wave periods of $\tau_{600THz}=\frac{5}{3}$ *fs* versus two 600 *THz* wavelengths of $\lambda_{600THz}=\frac{1}{2}$ micron has a space/time ratio that is a 3-figure round-off value c=$3.00\cdot10^8 m/s$ for speed of light.

$$\Delta x/\Delta t=\lambda_{600THz}\ /\tau_{600THz}=3.00\cdot10^8 m/s \simeq c=2.99792458\cdot10^8 m/s \tag{1}$$

Ken Evenson's light speed value c=299,792,458m/s became the international definition of the meter due in part to his post-lab efforts.

A horizontal space x-axis with a vertical time axis c-scaled to y=ct gives a +45° light wave trajectory $y=cx$ for Alice in Fig.1a and the opposite trajectory y=-cx for Carla's laser wave in Fig.1c. The geometric unit for either axis in Fig.1a-c is a half-wavelength $\frac{1}{2}\lambda_{600THz}=\frac{1}{4}$micron or else a half-period $\frac{1}{2}\lambda_{600THz}$= 5/6 fs. These apply as well to the real-wave-node grid Bob sees in Fig.1b.

We choose Alice's frequency υ=600THz=$6\cdot10^{14}$/s for arithmetic simplicity (Also for its beautiful Mediterranean blue-green color.) The frequency υ is divisible by c=$3.00\cdot10^8 m/s$ to give an integral wavenumber $\kappa=\upsilon$/c=$2\cdot10^6/m$, *i.e.* 2 million waves per (rounded-off) meter or 2000 per (rounded-off) millimeter or just 2 per micron. (Note for the record: Unrounded meter sticks hold 2001.384571 of real 600Tera-Hertz lightwaves in each 1-*millimeter* slot.) Fig.1d plots per-time units υ=300THz=$3\cdot10^{14}s^{-1}$ *vs* per-space units $\kappa_{300THz}=\upsilon_{300THz}/c=10^6 m^{-1}$ as is discussed next.

B. Per-space-time grid units

We learn physical units like *Joule* of energy, *Newton* of force by names of famous physicists. This is not the case for fundamental units of time (*second*) or distance (*meter*), although, after its 1980 metrological redefinition, one might call 1 *meter* an *Evenson.*

However, there are some more or less well established proper names for units of *per-space-time.* Most well known is the *Hertz* unit (1 *wave per second*=$1s^{-1}$) named after Heinrich

Hertz (1857-1894), an inventor of radio transmission. Less well known among atomic and molecular spectroscopists is the *Kayser* unit of (1 *wave per centimeter*=1cm^{-1}) named after Heinrich Kayser (1853-1940) an early solar spectroscopist who was born four years before Hertz and lived 46 years after him. We owe a lot to these two Heinrichs.

The horizontal axis of the per-space-time plot in Fig.1d is labeled by a Greek-k, that is, *kappa* (κ) defined by *wavenumber*=κ(waves per meter)=$\frac{1}{\lambda(meters\ \ per\ \ wave)}$. The angular equivalent k=$2\pi\kappa$ used to express phase is defined by *wavevector*=k=$2\pi\kappa$=*(radians)per meter*=$2\pi/\lambda$. The κ or k honor *Kayser*. Hertz frequency=υ=(waves per second) =$1/\tau$ has angular equivalent ω=$2\pi\upsilon$ for temporal phase defined by *angular frequency*=ω=$2\pi\upsilon$=(radians) per second. The letters υ and ω do not honor Hertz like Kayser's k. Instead, the Greek-n or nu(υ) (presumably for number) is most used. However, ν in most fonts resembles italic-v (ν) so we use υ (upsilon) for Hertz's per-second variable s^{-1} that gives frequency. (Now, Hertz might wonder why Greek H or eta (η) was never so employed.)

A c-scaled wavenumber-frequency (υ,cκ)-plot Fig.1d is the reciprocal of the space-time (x,ct) plot of Fig.1b and both preserve the $\pm45°$ c-lines for points representing laser CW. A more detailed (υ,cκ)-plot in Fig.2b underlies Bob and Alice using a Doppler shift in Fig. 2a to show why these c-lines are so special.

C. 1st order relativity: Doppler shifts and Evenson's c-Axiom

In Fig.2a, as in Fig.1a-b, Alice is providing Bob with a 600THz green CW laser beam, but she is doing it in a very sneaky (and expensive) way. Imagine she is millions of meters away in the figures and communicating by a super cell-phone with her laser on a space ship programmed to detune as she accelerates toward Bob by just enough to maintain a 600THz reading on Bob's spectrometer. At the moment shown she has paused her detuning and acceleration leaving her laser at infrared 300THz and her speed toward Bob at a high rate (to be calculated later) that blue-shifts 300THz to 600THz.

Supposing Bob's receiver is a precise atomic frequency υ-meter, Alice asks about wavelength λ or equivalently wavenumber κ=$1/\lambda$ that is a very different experiment involving fitting waves in space Δx rather than time interval Δt. We ask, Where on Bob's 600THz line ..,B,C,D,..in Fig.2b is his κ-reading? Could a B reading of κ=10^6m^{-1} happen and somehow reveal that Alice's light was a "phony"green born in a 300THz (that is κ=10^6m^{-1}) infrared

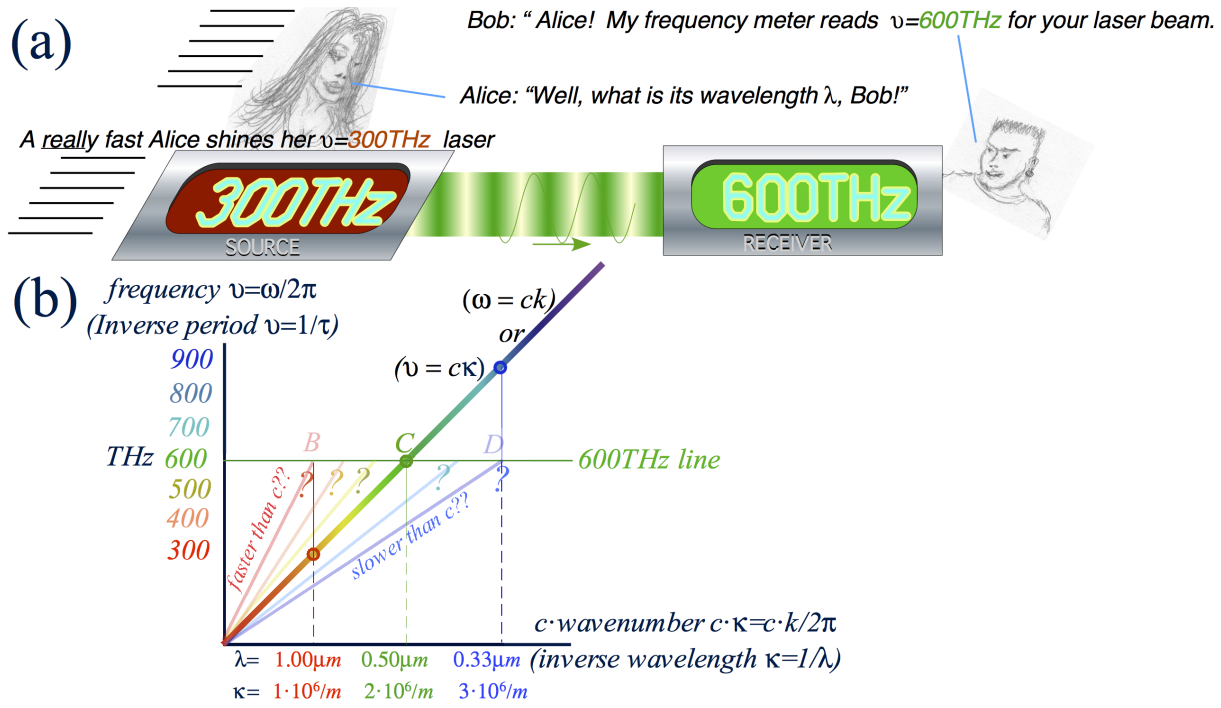

FIG. 2: (a) Alice sends Bob a 600THz that is an octave blue-shift of 300THz. (b) Is it a "phony"green? How could Bob tell?

laser? Or maybe a D reading of κ=3·10^{6}m^{-1} of a uv laser?

More to the point: How many kinds of this 600THz green can a spacetime vacuum support? It is either an infinite number or else just *one*. If we chose *one* then the answer here is C or (κ=2·10$^6 m^{-1}$) that belongs to Alice's original green with λ_{600THz}= $\frac{1}{2}$ *micron*=1/κ_{600THz}. Moreover, such uniqueness must hold for any color (frequency) that Alice sends to Bob: it has to lie on the 45° line through C in Fig.2b.

This forbids waves like B in Fig.2b having speed υ/κ faster than c or slower-than-c ones like D. It leads to what we will call Evenson's *c-Axiom: All CW colors go c en vacuo*. It is quite a retraction of Galileo's claim that adding Δu to your velocity subtracts Δu from all that surrounds you. Extra Δu along or against a CW will, respectively, down-tune (red-shift) or up-tune (blue-shift) equally both frequency υ and wavenumber κ so as to have zero effect on ratio υ/κ=c. If CW light colors march in lockstep we can resolve objects billions of light years away. But, if blue was even .01% slower than red, then it would arrive millions of years later than red and make a night sky with smears of chromatic aberrations.

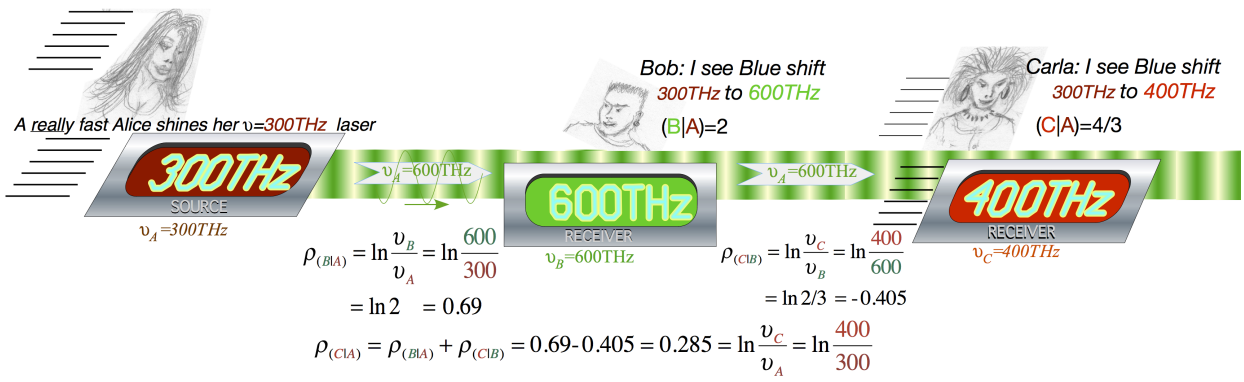

FIG. 3: Rapidity sum of Alice-Bob ρ_{BA} and Bob-Carla ρ_{CB} gives Alice-Carla ρ_{CA}.

1. *Doppler arithmetic and rapidity*

With frequency precision one can measure relative velocity by Doppler shift ratio (R|S).

$$(R|S) = \upsilon_{RECEIVER}/\upsilon_{SOURCE} \qquad \upsilon_{RECEIVER} = (R|S)\upsilon_{SOURCE} \tag{2}$$

If all frequencies go c (Evenson's axiom) a geometric frequency ratio is independent of υ_{SOURCE}. Not so for arithmetic difference υ_{RS}=$\upsilon_{RECEIVER}$-υ_{SOURCE}. Alice must detune her 2GHZ cell phone to 1GHz, the same factor (R|S)=2 that she detuned her 600THz laser to 300THz. (Or else, Bob will suspect she isn't the stay-at-home he had assumed. She also needs to attenuate her laser amplitude by that same factor as explained later.)

Geometric ratios suggest exponential-and-log-definitions by a variable called *rapidity* ρ_{RS}.

$$(R|S) = exp(\rho_{RS}) \qquad \rho_{RS} = ln(R|S) = \ln(\upsilon_{RECEIVER}) - \ln(\upsilon_{SOURCE}) \tag{3}$$

If ratio (R|S) is huge, ln(R|S) aids arithmetic, but the key use of ρ_{RS} is to simplify velocity addition to a Galilean sum. This is developed below following Fig. 3. First, note that (R|S) is a fraction R-over-S in (2a) with source S-denominator always on the right and read like Hebrew, right-to-left with source first as is the case for a Dirac bra-ket $\langle final|\, initial\rangle$. When υ_{SOURCE} exceeds $\upsilon_{RECEIVER}$ that will be a *red* shift (R|S)<1 with *negative* ρ_{RS}<0 due to R and S moving apart with *positive* radial velocity (quite like our stars and galaxies seeming not to like us). On the other hand *negative* rapidity ρ_{RS} means *positive* radial relative velocity. The opposite and more positive case (think of Carole and Bob getting together) involves a *blue* shift (R|S)>1 and *positive* ρ_{RS}>0 due to R and S moving *toward* each other.

Fig.3 is a view in Bob's frame with Alice approaching from the left at a high speed (indicated by slanted cartoon contrails) and Carla departing to the right at a lesser speed (shorter contrails). Alice's beam is drawn as a 600THz wave that Bob sees (Recall Fig. 2.) but is redshifted to 400THz according Carla's receiver. Digital readouts on Alice's source and receivers for Bob and Carla remain *invariant* if drawn for another frame, only appearance (color) of Alice's beam varies. Alice sees it as an infrared beam with the 300THz read-out of her source. Also frame-invariant: Doppler ratio (B|A), (C|B), (C|A) and rapidity $\rho_{(B|A)}$, $\rho_{(C|B)}$, or $\rho_{(C|A)}$ given by (3b). Bob's rapidity relative to Alice and Carla is as follows.

$$\rho_{(B|A)} = \ln \tfrac{v_B}{v_A} = \ln \tfrac{600}{300} = 0.69_{(Approaching)} \quad , \rho_{(C|B)} = \ln \tfrac{v_C}{v_B} = \ln \tfrac{400}{600} = -0.405_{(Separating)}$$

Rapidity for Bob-relative-to-Alice plus Carla-relative-to-Bob gives Carla-relative-to-Alice.

$$\rho_{(B|A)} + \rho_{(C|B)} = \ln \tfrac{v_B}{v_A} + \ln \tfrac{v_C}{v_B} = \ln \tfrac{v_B}{v_A}\tfrac{v_C}{v_B} = \ln \tfrac{v_C}{v_A} = \ln \tfrac{400}{300} = 0.69 - 0.405 = 0.285 = \rho_{(C|A)_{(Approach)}}$$

Galileo might be pleased to see his defunct v-sum-rule recover as a ρ-sum-rule. Doppler ρ is related below to classical v or u. Also effects of time reversal symmetry are used: Source becomes Receiver and *vice versa*, Doppler ratio inverts (R|S)→(S|R)=1/(R|S), and relative rapidity changes sign: $\rho_{(R|S)}$=-$\rho_{(S|R)}$.

III. SPACE-TIME COORDINATE GRIDS BY WAVE ZEROS

Fig.1b is a sum $e^{iR} + e^{iL}$ of Alice's right-going wave e^{iR} and Carla's left-going wave e^{iL}. In Fig.1a, e^{iR} phase R=kx-ωt goes right:x=$\frac{\omega}{k}t$+$\frac{R}{k}$. In Fig.1c, e^{iL} phase L=-kx-ωt goes left: x=-$\frac{\omega}{k}t$-$\frac{L}{k}$. Vectors **R** and **L** represent phases R and L in ($c\kappa$,v)-space of Fig.1d .

$$\mathbf{R} = \begin{pmatrix} v \\ c\kappa \end{pmatrix} = \begin{pmatrix} 2 \\ 2 \end{pmatrix} = \begin{pmatrix} \omega/2\pi \\ ck/2\pi \end{pmatrix} \text{(a)} \qquad \mathbf{L} = \begin{pmatrix} v \\ -c\kappa \end{pmatrix} = \begin{pmatrix} 2 \\ -2 \end{pmatrix} = \begin{pmatrix} \omega/2\pi \\ -ck/2\pi \end{pmatrix} \text{(b)} \quad (4)$$

Fig.1d plot has v-units of 300THz and wavenumber κ-units of 10^6 waves per meter. This matches wave-length λ-units of $\frac{1}{4}$*micron* and period τ-units of $\frac{5}{3}$*fs* in Fig.1b.

White-line zeros in Fig.1b are found by factoring the plane wave sum $e^{iR} + e^{iL}$ as follows.

$$\Psi_{sum} = e^{iR} + e^{iL} = e^{i\frac{R+L}{2}}\left(e^{i\frac{R-L}{2}} + e^{-i\frac{R-L}{2}}\right) = e^{i\frac{R+L}{2}} 2\cos\tfrac{R-L}{2} = \psi_{phase}\psi_{group} \qquad (5a)$$

$$= \psi_{phase}\psi_{group} = e^{-i\omega t} 2\cos kx \text{ where: } R = +kx - \omega t \text{ and: } L = -kx - \omega t \qquad (5b)$$

Fig.1b plots factored wave sum e^{iR}+e^{iL} . The phase factor Ψ_{phase} is x-independent.

$$\psi_{phase} = e^{i\frac{R+L}{2}} = e^{-i\omega t} = \cos\omega t - i\sin\omega t \qquad (5c)$$

Ψ_{phase} is modulated by a t-independent *group envelope factor* Ψ_{group} (green 2-sided cosine).

$$\psi_{group} = 2\cos\tfrac{R-L}{2} = 2\cos kx \tag{5d}$$

In (cκ,υ) space (Fig.1d) factors Ψ_{phase} and Ψ_{group} go with vectors **P** and **G**, respectively.

$$\mathbf{P} = \tfrac{\mathbf{R+L}}{2} = \begin{pmatrix} \upsilon \\ 0 \end{pmatrix} = \begin{pmatrix} 2 \\ 0 \end{pmatrix} = \begin{pmatrix} \frac{\omega}{2\pi} \\ 0 \end{pmatrix} \tag{5e}$$

$$\mathbf{G} = \tfrac{\mathbf{R-L}}{2} = \begin{pmatrix} 0 \\ c\kappa \end{pmatrix} = \begin{pmatrix} 0 \\ 2 \end{pmatrix} = \begin{pmatrix} 0 \\ \frac{ck}{2\pi} \end{pmatrix} \tag{5f}$$

Real wave zeros (Re $\psi_{phase}\psi_{group}$ =0) trace a square *(x,ct)* space-time grid in Fig.1b.

$$0 = \mathrm{Re}\psi_{phase} = \mathrm{Re}e^{i\frac{R+L}{2}} = \mathrm{Re}e^{-i\omega t} = \cos\omega t \text{ define horizontal t}-\text{lines } :t = \pm\tfrac{\pi}{2\omega}, \pm\tfrac{3\pi}{2\omega}... \tag{6a}$$

$$0 = \mathrm{Re}\psi_{group} = \mathrm{Re}e^{i\frac{R-L}{2}} = \mathrm{Re}e^{-ikx} = \cos kx \text{ define vertical } x-\text{lines } :x = \pm\tfrac{\pi}{2k}, \pm\tfrac{3\pi}{2k}... \tag{6b}$$

The*(x,ct)* coordinate lines mark half-periods $\frac{\tau}{2}=\frac{\pi}{\omega}=\frac{1}{2\upsilon}$ and half-wavelengths $\frac{\lambda}{2}=\frac{\pi}{k}=\frac{1}{2\kappa}$ that lie mid-way between crests (lighter regions) and troughs (darker regions) in Fig. 1b. The real part of each wave snapshot in Fig.1a-c is plotted in dark blue while its imaginary part is plotted in cyan. The latter always leads by 90° in phase. A corporate aphorism *Imagination precedes Reality by one Quarter* holds dearly for these waves or for any harmonic oscillation.

Group envelope zeros trace vertical coordinate lines parallel to $\mathbb{G}$ in Fig.1b. They have zero x-velocity of a standing wave. This corresponds to a Group **G**-vector with zero slope in the (υ,cκ) plot of Fig.1d. The Phase **P**-vector in Fig.1d has infinite slope. This indicates an infinite velocity along the $\mathbb{P}$ vector in *(x,ct)* plot Fig.1b for ReΨ_{phase} zeros that happen every $\frac{1}{2}$-period. Bob sees two "instantons" zip by in each period of $\tau_{phase}=\frac{5}{3}10^{-15}s=\frac{5}{3}fs$ due to the colliding 600THz waves provided by Alice and Carla.

Bob's (υ,cκ) plot in Fig.1d is what we call a *Relawavity Baseball-Diamond* (RBD). Origin is *home-plate*, the **R**-vector is the *1st-baseline*, the **L**-vector is the *3rd-baseline*, **R**+**L** points to *2nd-base*. Phase **P** points to *Pitcher's mound*. Group **G** points to a *Grandstand*.

G and **P** vectors of reciprocal spacetime (υ,cκ) Fig.1d trade positions in Bob's spacetime *(x,ct)* plot of Fig.1b. Zero group wave velocity is indicated by a vertical vector $\mathbb{G}$. Its length is period τ. Phase wave velocity (∞ here) is indicated by a horizontal vector $\mathbb{P}$ whose length is wavelength λ. Together, $\mathbb{G}$ and $\mathbb{P}$ define a 2-by-2 square with 2 wave crests and 2 wave troughs in each space-time lattice unit cell.

A. Wave zeros trace Minkowski lattices

Bob sees warped cells if Alice and Carla have velocity u relative to him or equivalently if he has velocity -u relative to them. Resulting Doppler effects are diagrammed in Fig. 4.

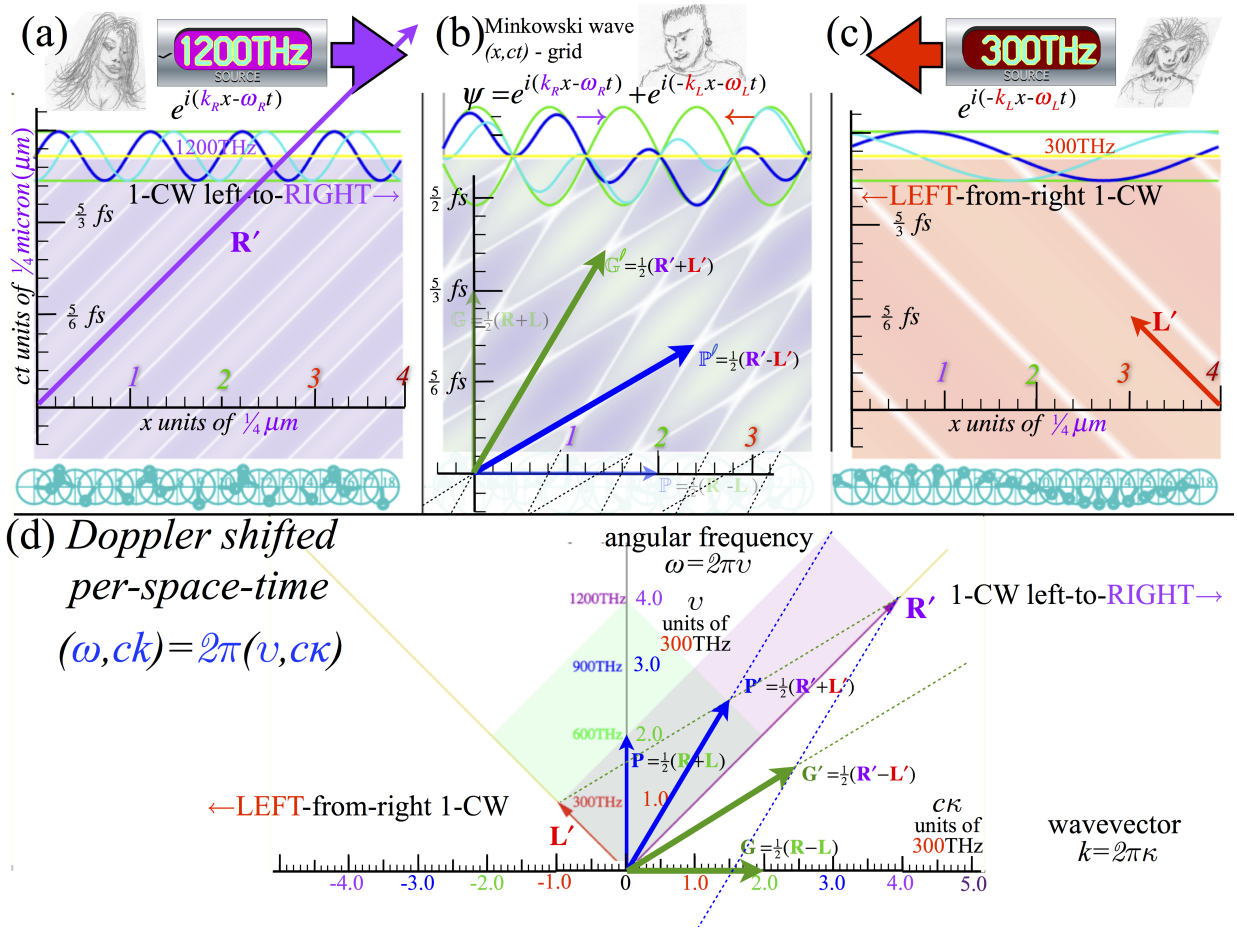

FIG. 4: *(x,ct)* wave plots (a) Alice's **R′**-CW (b) Bob's Group **G′** over Phase **P′** (c) Carla's **L′**-*CW* (*d*)(*cκ*,*υ*) plots of **P′** over **G′**

Bob sees Alice's υ_A=600THz laser beam blue-shifted due to her speed (derived later) toward him. So a vector that Bob plots in Fig. 4d for Alice is her original vector $\mathbf{R} = \upsilon_A \binom{1}{+1}$ *doubled* in length by the blue shift to $\mathbf{R}' = (B|A)\upsilon_A \binom{1}{+1} = \upsilon_A \binom{2}{+2}$ along the 1st-base line (45°). Her waves run head-on into Carla's υ_C=600THz beam that Bob sees red-shifted by $(B|C) = e^{-\rho_{BC}} = \frac{1}{2}$ due to Carla's speed away from Bob. So her original vector $\mathbf{L} = \upsilon_A \binom{1}{-1}$ is *halved* in length to $\mathbf{L}' = r_{BC}\upsilon_A \binom{1}{-1} = \upsilon_A \binom{\frac{1}{2}}{-\frac{1}{2}}$ along 3rd-base line (-45°). Here Evenson's axiom confines 1-CW light to the 1st-base line for positive κ and to the

3rd-base line for negative κ. (Baseball rule: A 1-CW must run in its baseline!)

Alice's right-going vector $\mathbf{R}$ (Bob's view $\mathbf{R}'$) and Carla's left-going vector $\mathbf{L}$ (Bob's view $\mathbf{L}'$) enter a half-sum $\mathbf{P}=\frac{1}{2}(\mathbf{R}+\mathbf{L})$ in(5e). Bob's view is:$\mathbf{P}'=\frac{1}{2}(\mathbf{R}'+\mathbf{L}')$ for the phase factor.

$$\mathbf{P}'=\begin{pmatrix} \upsilon'_{phase} \\ c\kappa'_{phase}\end{pmatrix}=\tfrac{1}{2}(\mathbf{R}'+\mathbf{L}')=\upsilon_A\begin{pmatrix}\frac{1}{2}(e^{\rho}+e^{-\rho})\\ \frac{1}{2}(e^{\rho}-e^{-\rho})\end{pmatrix}=\upsilon_A\begin{pmatrix}\cosh\rho\\ \sinh\rho\end{pmatrix}=\upsilon_A\underset{Bob's\ View}{\begin{pmatrix}\frac{5}{4}\\ \frac{3}{4}\end{pmatrix}}\ \text{or :}\upsilon_A\underset{Alice's\ View}{\begin{pmatrix}1\\0\end{pmatrix}} \tag{7a}$$

Group wave factor of (5f) belongs to $\mathbf{G}=\frac{1}{2}(\mathbf{R}-\mathbf{L})$ Bob's view of $\mathbf{G}$ is $\mathbf{G}'=\frac{1}{2}(\mathbf{R}'-\mathbf{L}')$.

$$\mathbf{G}'=\begin{pmatrix} \upsilon'_{group} \\ c\kappa'_{group}\end{pmatrix}=\tfrac{1}{2}(\mathbf{R}'-\mathbf{L}')=\upsilon_A\begin{pmatrix}\frac{1}{2}(e^{\rho}-e^{-\rho})\\ \frac{1}{2}(e^{\rho}+e^{-\rho})\end{pmatrix}=\upsilon_A\begin{pmatrix}\sinh\rho\\ \cosh\rho\end{pmatrix}=\upsilon_A\underset{Bob's\ View}{\begin{pmatrix}\frac{3}{4}\\ \frac{5}{4}\end{pmatrix}}\ \text{or :}\upsilon_A\underset{Alice's\ View}{\begin{pmatrix}0\\1\end{pmatrix}} \tag{7b}$$

Slope of Bob's group vector $\mathbf{G}'$ in (cκ,υ)-plot of Fig.4d is group wave velocity in c-units.

$$\frac{V^{group}}{c}=\frac{\upsilon'_{group}}{c\kappa'_{group}}=\frac{\sinh\rho}{\cosh\rho}=\tanh\rho=\frac{\frac{3}{4}}{\frac{5}{4}}=\frac{3}{5}\equiv\frac{u}{c}\equiv\beta \tag{8a}$$

This is the speed $\frac{u}{c}=\frac{3}{5}$ of Alice and Carla's *group* or *envelope* wave in Bob's space-time plot of Fig. 4b. u/c is the conventional relativity parameter $\beta\equiv\frac{u}{c}$ for velocity of Alice and Carla relative to Bob. For Alice or Carla this group wave is a *standing* wave held by their laser cavities. Fig.4b also shows a much faster *phase* or *carrier* wave that Bob would (if he could!) record going $\frac{5}{3}$ faster than light, always the inverse of the group wave speed..

$$\frac{V^{phase}}{c}=\frac{\upsilon'_{phase}}{c\kappa'_{phase}}=\frac{\cosh\rho}{\sinh\rho}=\coth\rho=\frac{\frac{5}{4}}{\frac{3}{4}}=\frac{5}{3}\equiv\frac{c}{u}\equiv\frac{1}{\beta} \tag{8b}$$

Noted before in Fig.1b were "instantons" seen by Bob to have infinite phase velocity. Bob sees a slower phase velocity (8b) in Fig.4b. Close examination of Fig.4b or Fig.5b reveals several phase-zero white lines intersecting the dark blue wave curves near the top of the figure at which point they are going at the super-luminal speed of $\frac{u}{c}=\frac{5}{3}$ ($\mathbb{P}'$ slope is $\frac{5}{3}$ off of the x'-axis in Fig.5b as $\mathbf{P}'$ slope is $\frac{5}{3}$ off of the cκ'-axis in reciprocal space of Fig.4d or Fig.5a. (Per-space-time ($\mathbf{P}'$,$\mathbf{G}'$) vectors invert into ($\mathbb{G}'$,$\mathbb{P}'$) vectors in space-time.)

Fig.5a details Bob's (cκ,υ)-plot of Fig.4d. Fig.5b details Bob's *(x,ct)*=(λ,cτ)-plot in Fig.4b. The (cκ,υ)-coordinates (7a) of $\mathbf{P}'$ are $c\kappa_{phase}=c/\lambda_{phase}$ and $\upsilon_{phase}=1/\tau_{phase}$ and (cκ,υ)-coordinates (7b) of $\mathbf{G}'$ give $c\kappa_{group}=c/\lambda_{group}$ and $\upsilon_{group}=1/\tau_{group}$ in Alice units that are υ_A=600THz in Fig.5a. In Fig.5b her x-units and ct-units are $\frac{1}{2}$ micron: $\upsilon_A=(0.5{\cdot}10^{-6}m)$. The interval between successive intercepts of $\mathbb{P}'$-lines (or $\mathbb{G}'$-lines) with Bob's space x'-axis is half-wavelength $\frac{1}{2}\lambda_{phase}$ (or $\frac{1}{2}\lambda_{group}$). Corresponding intercepts with

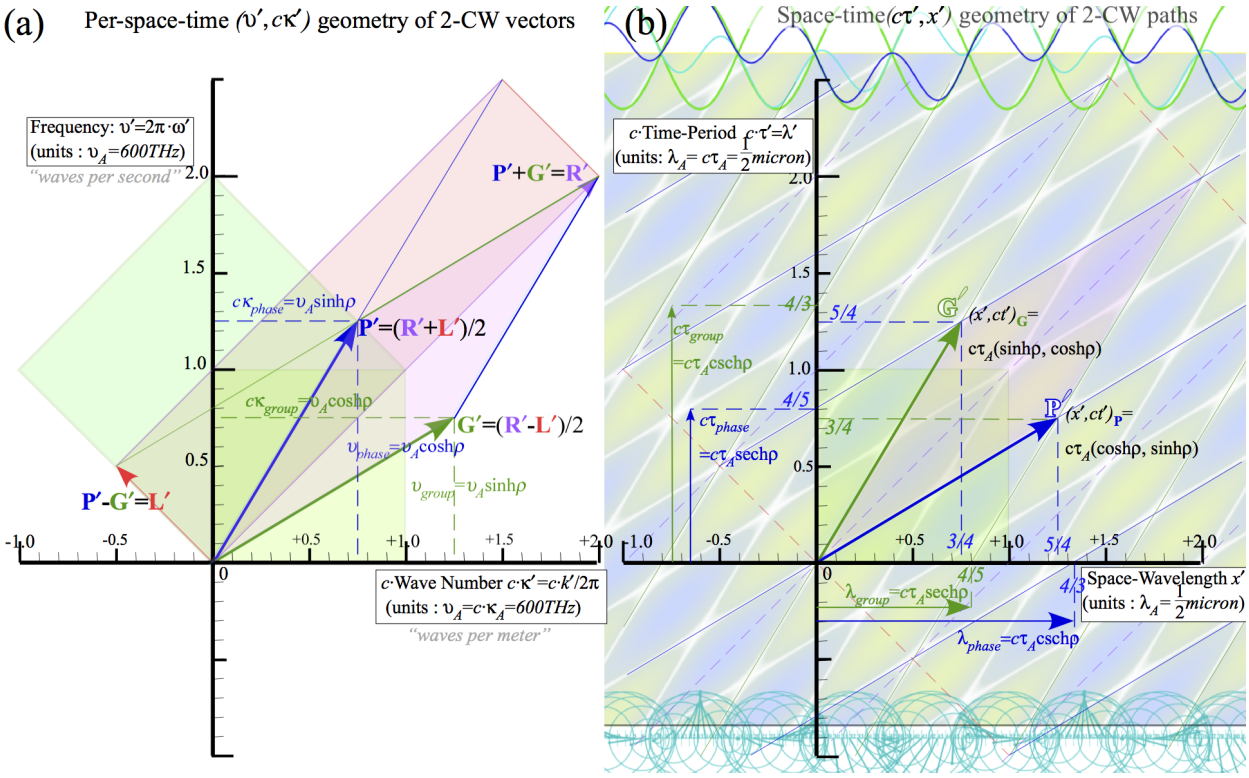

FIG. 5: Relawavity parameters given as ρ-functions as they appear in (a) Per-space-time and (b) Space-time

time ct'-axis is half-period $\frac{1}{2}\tau_{phase}$ (or $\frac{1}{2}\tau_{group}$). These eight quantities, two wave velocities (V_{phase} and V_{group}) and two Doppler shifts ($e^{+\rho}$ and $e^{-\rho}$) appear in eight columns of Table I showing their dependence on rapidity ρ, stellar aberration σ (defined below), and the old-fashioned relativity parameter $\beta=\frac{u}{c}$. Numerical values are in the last row for the case $\beta=\frac{u}{c}=\frac{3}{5}$ for examples done so far. The number in 1^{st} column($\frac{1}{2}$=0.5) inverts in 8^{th} column($\frac{2}{1}$=2.0), 2^{nd} column($\frac{3}{5}$=0.6) inverts in the 7^{th}($\frac{5}{3}$=1.67), and so forth.

B. Spatial and temporal wave-warping at warp-speed 3c/5

In Table I six coefficients (excluding Doppler exponentials $e^{\pm\rho}$) give shrinkage or expansion ratios seen by Bob to affect Alice's spatial and temporal geometry. The first two, $\tanh\rho$ and $\sinh\rho$, are (like Doppler) 1^{st}-order in rapidity ρ and first observable at terrestrial speeds $u \ll c$ where both (and ρ) approximate the old-fashioned relativity parameter $\beta = u/c$. As derived in (8a) $\tanh\rho$ is exactly equal to β.

phase	$b^{Doppler}_{RED}$	$\frac{c}{V_{phase}}$	$\frac{\kappa_{phase}}{\kappa_A}$	$\frac{\tau_{phase}}{\tau_A}$	$\frac{\upsilon_{phase}}{\upsilon_A}$	$\frac{\lambda_{phase}}{\lambda_A}$	$\frac{V_{phase}}{c}$	$b^{Doppler}_{BLUE}$
group	$\frac{1}{b^{Doppler}_{BLUE}}$	$\frac{V_{group}}{c}$	$\frac{\upsilon_{group}}{\upsilon_A}$	$\frac{\lambda_{group}}{\lambda_A}$	$\frac{\kappa_{group}}{\kappa_A}$	$\frac{\tau_{group}}{\tau_A}$	$\frac{c}{V_{group}}$	$\frac{1}{b^{Doppler}_{RED}}$
rapidity ρ *stellar* $\measuredangle$ σ	$e^{-\rho}$	$\tanh\rho$ $\sin\sigma$	$\sinh\rho$ $\tan\sigma$	$\operatorname{sech}\rho$ $\cos\sigma$	$\cosh\rho$ $\sec\sigma$	$\operatorname{csch}\rho$ $\cot\sigma$	$\coth\rho$ $\csc\sigma$	$e^{+\rho}$
$\beta\equiv\frac{u}{c}$	$\sqrt{\frac{1-\beta}{1+\beta}}$	$\frac{\beta}{1}$	$\frac{1}{\sqrt{\beta^{-2}-1}}$	$\frac{\sqrt{1-\beta^2}}{1}$	$\frac{1}{\sqrt{1-\beta^2}}$	$\frac{\sqrt{\beta^{-2}-1}}{1}$	$\frac{1}{\beta}$	$\sqrt{\frac{1+\beta}{1-\beta}}$
value for β=3/5	$\frac{1}{2}$= 0.5	$\frac{3}{5}$=0.6	$\frac{3}{4}$=0.75	$\frac{4}{5}$=0.80	$\frac{5}{4}$=1.25	$\frac{4}{3}$=1.33	$\frac{5}{3}$=1.67	$\frac{2}{1}$=2.0

TABLE I: Relawavity variables and dependency on rapidity ρ, stellar angle σ, and velocity u=βc (for $\beta=\frac{3}{5}$)

$$\beta \equiv \frac{u}{c} = \tanh\rho \xrightarrow[u\ll c]{} \rho \text{ or } :\beta \tag{9a}$$

$$\frac{\upsilon_{group}}{\upsilon_A} = \sinh\rho = \frac{1}{\sqrt{\beta^{-2}-1}} = \frac{\beta}{\sqrt{1-\beta^2}} \xrightarrow[u\ll c]{} \beta \text{ or } :\rho \tag{9b}$$

These two order-1 coefficients describe the biggest relativistic effects. First, is relative velocity itself that is slope tanhρ. It is *wave group velocity* V_{group}=c tanhρ and slope of Alice's time ct-axis (x=0.)versus Bob's ct'-axis. Second, sinhρ gives slope tanhρ= of Alice's space x-axis in Fig. 5b (that is: ct=0) versus Bob's x'-axis (that he calls ct'=0). This past-future asynchrony lets Bob see into Alice's past (t<0) as he waits for her to pass his origin (x'=0), and to see into her future (t>0) after she passes. Now the next two coefficients, sechρ and coshρ, are order-2 effects and tiny at normal speeds, but Table I is not normal. (At speed needed for e^{ρ}=2 we circle Earth in a $\frac{1}{4}$-second.) These are ratios for Lorentz length-contraction and Einstein time-dilation that sophomore students learn.

$$\frac{\lambda_{group}}{\lambda_A} = \operatorname{sech}\rho = \sqrt{1-\beta^2}\Big|_{\frac{u}{c}=\beta=\frac{3}{5}} = \frac{4}{5} = 0.8 \tag{10a}$$

$$\frac{\upsilon_{phase}}{\upsilon_A} = \cosh\rho = \frac{1}{\sqrt{1-\beta^2}}\Big|_{\frac{u}{c}=\beta=\frac{3}{5}} = \frac{5}{4} = 1.25 \tag{10b}$$

λ_{group} in Fig.5b lies between two speed grid lines, one along $\mathbb{G}'$ and the other just hitting the tip of phase $\mathbb{P}'$ vector after crossing Bob's x'-axis at x'=4/5. That shows an 80% contraction from unit distance (λ_A=λ_{600THz}=$\frac{1}{2}$micron) down to $\frac{2}{5}$micron=0.4μm. (We ignore $\frac{1}{2}$-wave nodal lines and measure the full wavelength λ.)

A critically thinking student may ask if the 80% "squish"of the $0.5\mu m$ group light wave down to $0.4\mu m$ would also apply to its $0.5\mu m$ Invar-steel optical cavity. Indeed, the cavity must also "squish" by *exactly* 80% in order to maintain resonance!. Here *Relawavity* gets serious as it seems that *everything* obeys such wave mechanical rules of distortion. This leads to derivation of quantum wave mechanical rules. There QM phase frequency turns out to be astronomically high. (Yet, the ratios of Table I apply to *all* frequencies.)

Remaining wave dimensions λ_{phase} and τ_{group} vary as cschρ from infinity at ρ=0 to finite values as $\rho\rightarrow\infty$. Recall the Alice-Carla standing wave phase has *infinite wavelength* while its group has *infinite period*. The Einstein time dilation (10b) is better stated as time *slowing* experienced by moving Alice as Bob compares his reading of phase frequency to her v_A=600THz laser or else his reading of wave time period to her τ_A=$\frac{5}{3}$fs. Along the vertical axis of Fig. 5b, $c\tau_{phase}$ is marked-down by 4/5 so Bob sees an 80% period-*contraction*. That is a 125%=5/4 frequency *increase* relative to what Alice sees. It is indicated by v_{phase}-coordinate 1.25 of $\mathbf{P}'$-vector in Fig. 5a or 750THz.

Another way to mark time-slowing uses the tip of vector $\mathbb{G}'$ in space-time plot Fig.5b where Bob sees Alice passing her unit (ct_A=1.0) time line just as she also passes Bob's 5/4-line (ct'=1.25). So Bob says she ticks 4/5 slower than he does using either space-time and per-space-time views. If Bob arranges to provide a 2-laser grid surrounding Alice, then she observes Lorentz contraction, **(P,G)** inclination, and phase slowing, similar to Fig.5 only now with Bob's velocity to the left. So both Bob and Alice claim the other has lagging clocks and shriveled meter sticks. This lovers'-quarrel is made less paradoxical by replacing "clocks" and "meter-sticks" by light wave geometry. Then it is no more paradoxical than both seeing the same shriveled (red) Doppler frequency shift $e^{-|\rho|}$ of the other's laser when moving apart ($\rho>0$) or the same positive blue shift $e^{+|\rho|}$ when approaching ($\rho<0$).

C. Thales mean geometry and hyperbolic trigonometry

A re-analysis of Alice-Bob-Carla laser thought experiment is instructive. Suppose again Bob detects counter-propagating laser beams of frequency ω_R going left-to-right (due to Alice's laser) and ω_L going right-to-left (due to Carla's laser). Two questions arise:

(1.) To what velocity u_E must Bob accelerate so he sees beams with equal frequency ω_E?

(2.) What is that frequency ω_E?

Query (1.) has Jeopardy style answer-by-question: What group velocity does Bob see?

$$u_E = V_{group} = \frac{\omega_{group}}{k_{group}} = \frac{\omega_R - \omega_L}{k_R - k_L} = c\frac{\omega_R - \omega_L}{\omega_R + \omega_L} \text{ where } :\omega_R{=}ck_R, \text{and } \omega_L{=}-ck_L \tag{11}$$

Query (2.) similarly: What ω_E is blue-shift $b\omega_L$ of ω_L and red-shift ω_R/b of ω_R?

$$\omega_E = b\,\omega_L = \omega_R/b \;\Rightarrow\; b = \sqrt{\omega_R/\omega_L} \;\;\Rightarrow\;\; \omega_E = \sqrt{\omega_R \cdot \omega_L} \tag{12}$$

V_{group}/c is ratio of difference-mean $\omega_{group} = \frac{\omega_R - \omega_L}{2}$ to arithmetic-mean $\omega_{phase} = \frac{\omega_R + \omega_L}{2}$. Frequency $\omega_E{=}B$ is the geometric mean $\sqrt{\omega_R \cdot \omega_L}$ of left and right-moving frequencies defining the geometry in Fig.6 as detailed in Fig.6a. Line sum of $\omega_L = \omega_E e^{-\rho}$ and $\omega_R = \omega_E e^{+\rho}$ is bisected at center C of a circle connecting shifted phase vector $\mathbf{P'}$ to its $\sqrt{\omega_R \cdot \omega_L}$ original $\mathbf{P}$ (Pitcher's mound) at the geometric mean point for Alice's base frequency of $B{=}\upsilon_A{=}$600THz. (Fig.6 units are 300 THz.).

We construct points $\mathbf{P'}$, $\mathbf{P''}$, $\mathbf{P'''}$,... on a hyperbola in Fig.6b that all frames use to mark their 600 THz tic. Geometry begins by choosing to prick a C'-point ck' with compass needle. Then compass pencil is set to point-$\mathbf{P}$, and p-Circle arc $\mathbf{P'P}$ is drawn to locate hyperbola point $\omega'(k')$ over C'-point ck'. (Arc is optional if vertical graph grid fixes $\mathbf{P'C'}$ line.) Group hyperbola points $\mathbf{G'}$, $\mathbf{G''}$, $\mathbf{G'''}$,... are made similarly.

1. *Trigonometric Road Maps (TRM)*

The preceding top-down relativity development (physics before math) is paused to compare a bottom-up approach. It begins with geometry and trigonometry of both hyperbola and circle. (In this it matches 1st year physics students reviewing sines and cosines but in

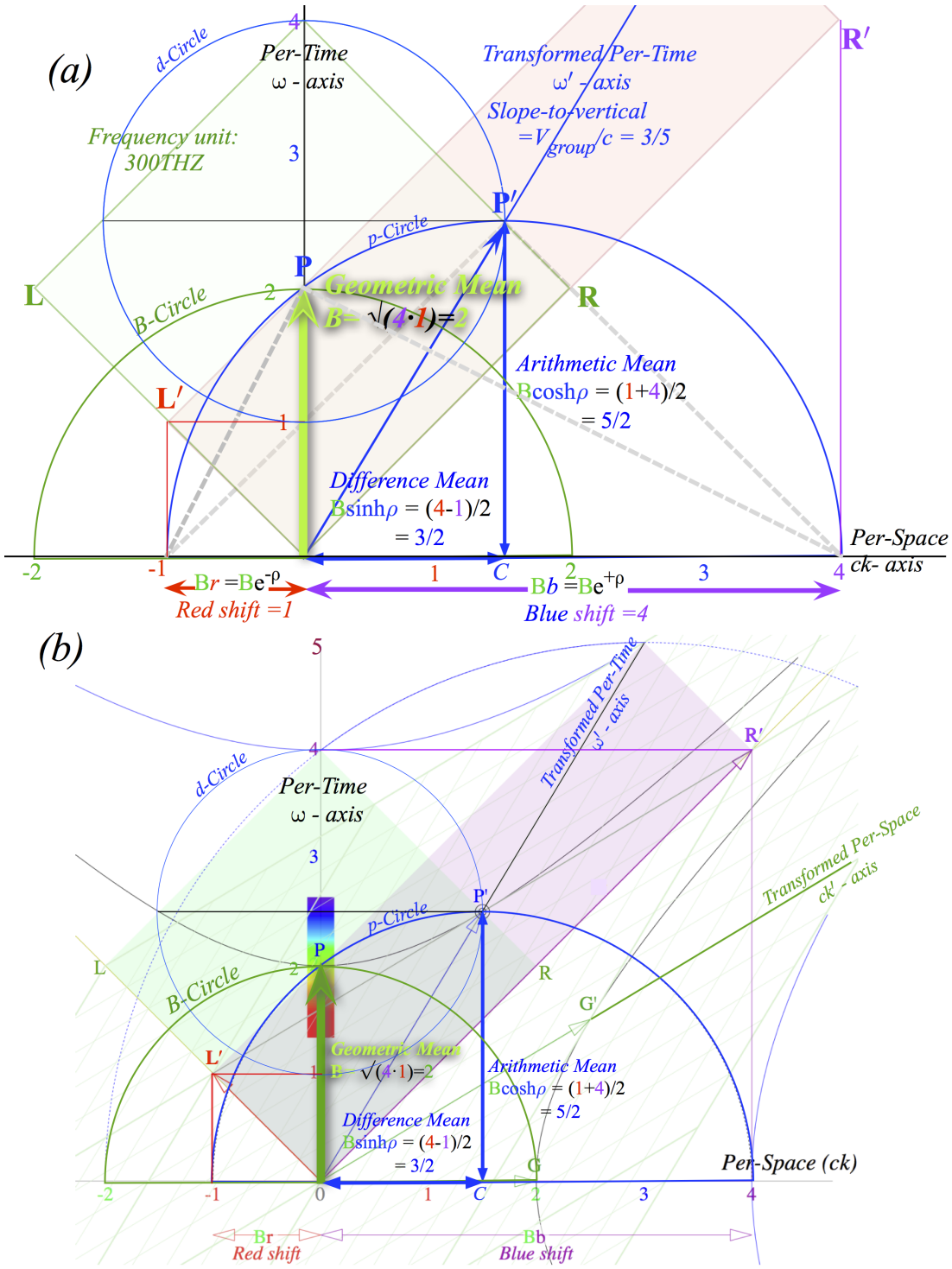

FIG. 6: (a) Thales-Euclid geometric, difference, and arithmetic means (b) Hyperbola construction step by circle radius **CP'**

an unusual way.) As it turns out, it is easier to do algebra of hyperbolic functions *before*

circular ones and the two have identical geometric "road-maps"(connection diagrams) shown in Fig.7. This displays all functions in Table I as fractions made of sides of inter-lapped 3:4:5 triangles as per Doppler shift $e^{\rho} = 2$ or rapidity $\rho = \ln 2 = 0.6931$.

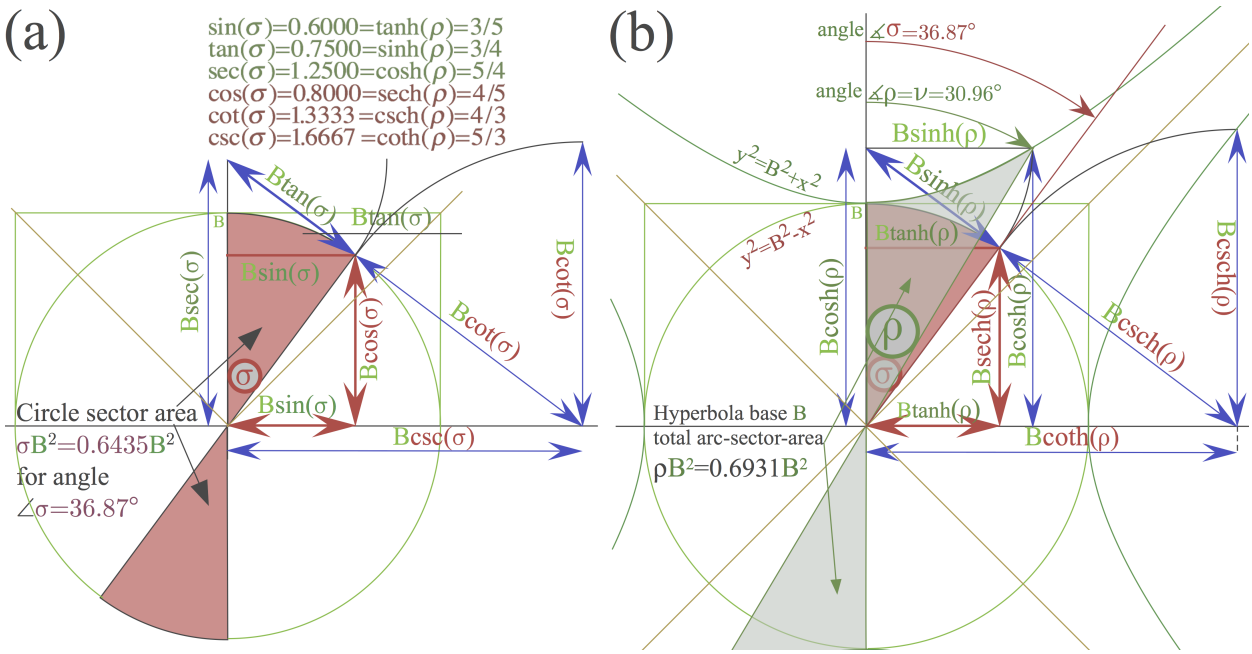

FIG. 7: (a) Circular functions of total sector area σ.
(b) Hyperbolic functions of total hyper-sector area ρ.

Instead of angles, both figures vary with diameter-swept area σ for the circle in Fig.7a and ρ for the hyperbola in Fig.7b. The circle's σ is the usual angle in radians. (Unit radius sweeps π of arc while diameter sweeps up π of area.) The hyperbola has no arc-radian equivalent but counts diameter-swept area ρ as diametrically-opposite ends follow points on opposite branches. Unit radii (B=1) are assumed. To compare the basic TRM of Fig.7b to Fig.6 some tangent lines and their intercepts are added to give Fig.8 below. This also has points labeled as they are in Fig.6. In particular there is the Right-Doppler k-point **R**, the Left-Doppler k-point **L**, and the phase point **P** in between, and all three lie on a tangent line to hyperbola at **P** that intersects the horizontal axis at I_P. A similar tangent line thru **R** and group tangent point **G** to below where it intercepts vertical axis at I_G. The slopes of these lines are respectively, $\tanh\rho$ and $\coth\rho$, the group velocity and phase velocity functions in Table I, an interesting case where derivative $\frac{d\omega}{dk}$ at **P** is exactly equal to discrete difference $\frac{\Delta\omega}{\Delta k} = \frac{\omega_R - \omega_L}{k_R - k_L}$.

Of particular interest is the B-circle tangent line contact point **S** where the *d-circle* of radius $B\sinh\rho$ (the difference-mean) is tangent to a circle of radius $B\text{csch}\rho$. That tangent line slope (-sinhρ) also equals (-tanσ) by Table I and so is normal to stellar aberration radius **OS** at angle σ to the vertical. The rapidity parameter ρ involves light moving longitudinally or *parallel* to direction of relative velocity $u{=}c\tanh\rho$. Stellar aberration angle σ is between light beam and a *normal* to direction of relative velocity $u{=}c\sin\sigma$ and leads to a *transverse* view of relativity pioneered by Epstein. Details of this approach are in following sections.

In Fig.8 hyperbolic functions define points $(x,y){=}(\sinh\rho,\ \cosh\rho)$ on unit hyperbola $y^2{=}{\pm}1^2{+}x^2$ in analogy to points $(x,y){=}(\sin\sigma,\ \cos\sigma)$ on unit circle $y^2{=}{\pm}1^2{-}x^2$. Here (x,y) is space-time (x,ct) of Fig. 5b or per-space-time $(ck,\omega){=}2\pi(c\kappa,)$ in Fig. 5a. There **P** and **G** hyperbola belong to various radii $B_0{=}\omega_0{=}ck_0$. A **P**-hyperbola exists for each *proper frequency* ω_0 and a **G**-hyperbola for *proper-k_0-vector* $k_0{=}\omega_0/c$.

In space-time Fig.5b a $\mathbb{G}$-hyperbola exists for each proper time τ_0 and a $\mathbb{P}$-hyperbola exists for each proper-distance $x_0{=}c\tau_0$. It is important to relate and yet distinguish the per-space-time hyperbolas $\omega(k)$ that are ω_0-*dispersion functions* from the space-time invariant hyperbolas that track proper x_0 and τ_0 grid-tics for any relative velocity.

$$\omega(k) = \pm\sqrt{\omega_0^2 + c^2k^2}\ \ \omega(\mathbf{P}) - \text{dispersion}\quad \text{(a)} \qquad x = \pm\sqrt{x_0^2 + c^2t^2}\quad \text{(b)} \tag{13}$$

Proper time τ_0 is an object's "own-time" or *age*. By zooming about we don't age as much! (See Fig.10 in the following sub-section.) Entering gravity fields slows aging proportionally. (Still a bit of a mystery.) Similarly, proper distance is an object's own dimension or *size*. As noted before this becomes reduced (Lorentz-contracted) by relative motion

D. Space-proper-time plots and stellar-aberration angle

Lewis C. Epstein[1] developed a novel approach to space-time relativity that uses the transverse stellar aberration angle σ to define relative velocity by $u = c\sin\sigma$ as sketched in Fig. 9. It is an alternative to longitudinal form $u = c\tanh\rho$ in terms of rapidity ρ in Doppler factor e^{ρ} that was derived in (8a). Epstein's alternative to Minkowski-(x,ct)-plots involves choosing between proper-time definitions (2a). Instead of the hyperbolic form he picks the Cartesian Pythagorean form:

$$(c\tau)^2 = (ct')^2 - (x')^2 \Rightarrow (c\tau)^2 + (x')^2 = (ct')^2 \tag{14}$$

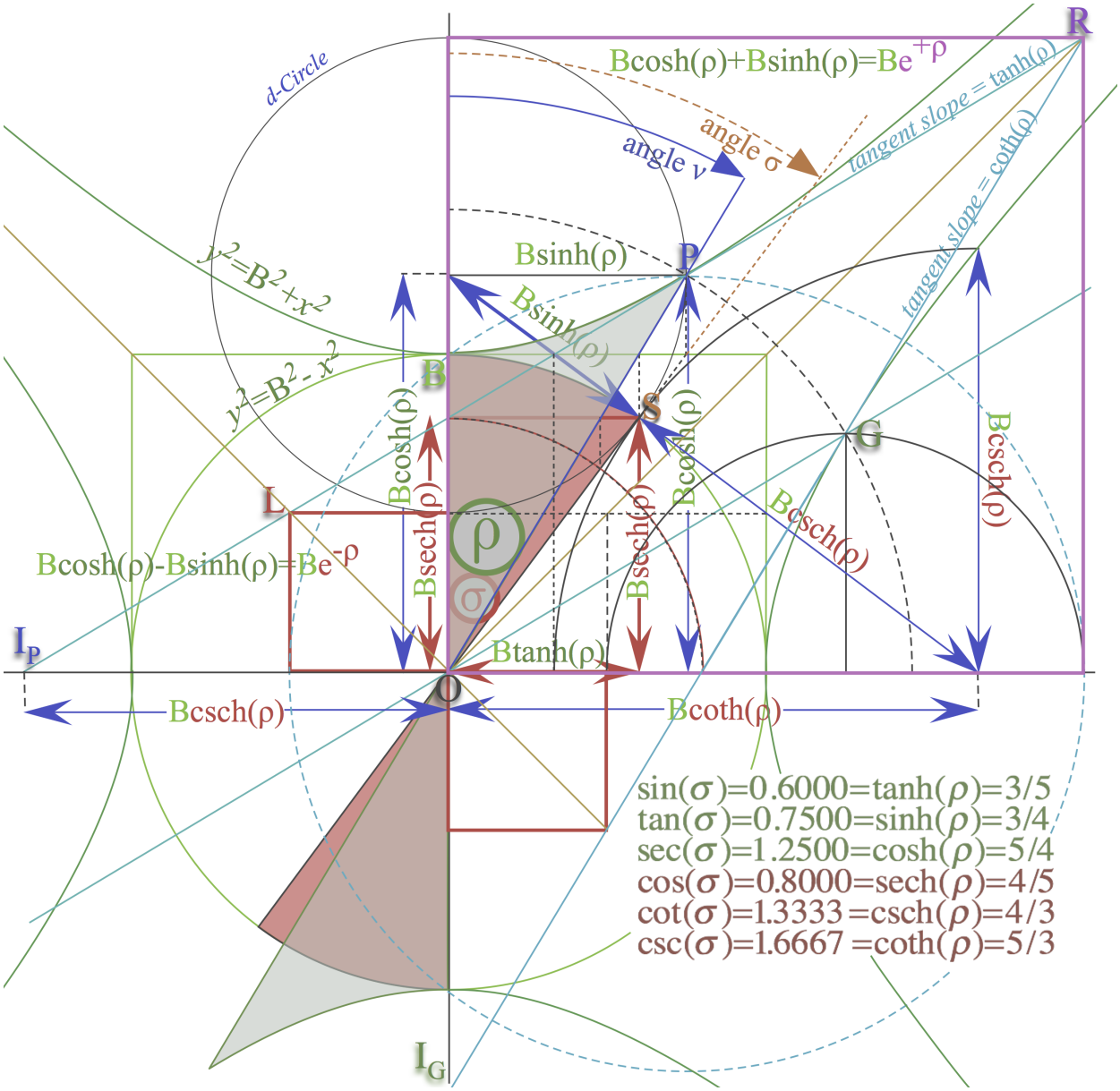

FIG. 8: More detailed TRM expanding hyperbolic labeling of Fig. 6 to include tangent lines.

A Pythagorean geometry for space-proper-time or $(x,c\tau)$-plots is shown by Fig.10. There it is imagined all things travel at light-speed c including a stationary object $(x' = 0)$ that "moves" parallel to the $(c\tau)$-axis at light speed c. The moving object P is indicated by a vector (ct') that is inclined at aberration angle σ and also grows at rate c as given by (14) with $(x' = u \cdot t')$. Then circular σ-functions describe the time dilation $(\sec\sigma)$, length contraction $(\cos\sigma)$, and time asynchrony $(\sin\sigma)$ that were previously given in terms of hyperbolic ρ-

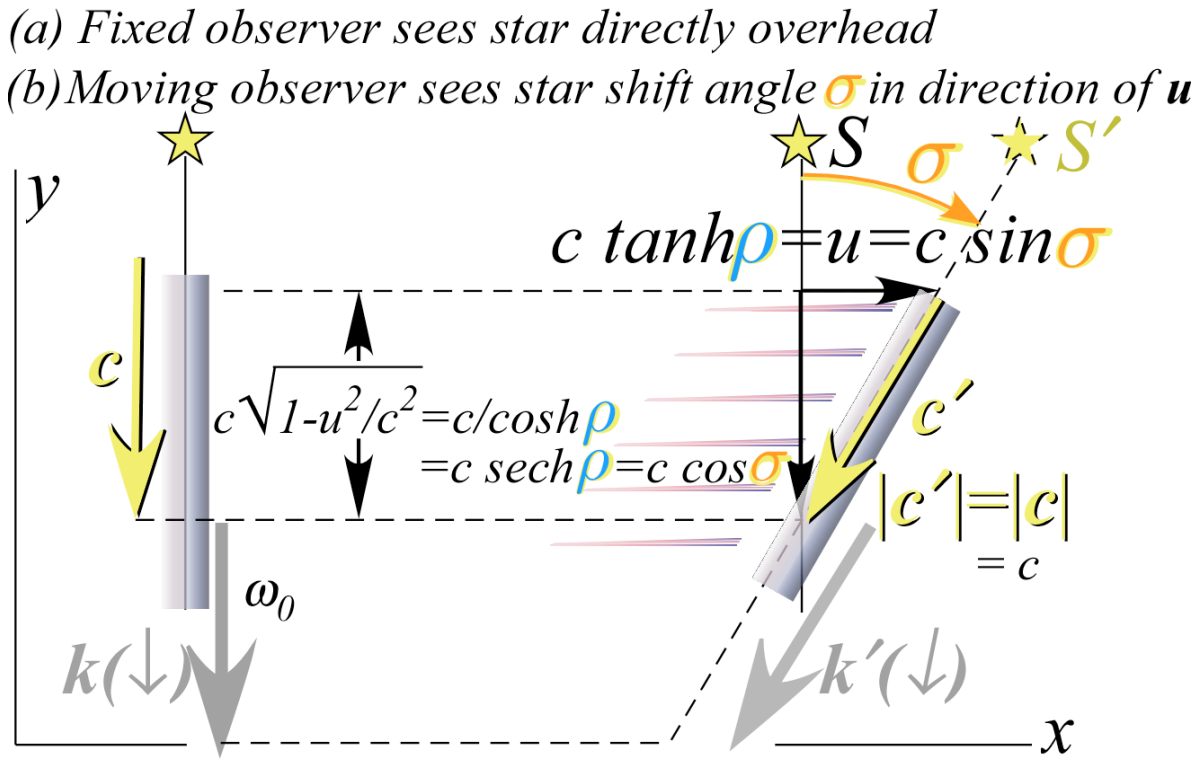

FIG. 9: Stellar aberration angle σ of light beam normal to direction of velocity u.

functions (coshρ), (sechρ), and (sinhρ) in (9) and (10). Epstein plots are better for analyzing twin-paradox scenarios. Note how proper time $c\tau$ drops to zero as u nears c. (Light cannot age!) *(x,cτ)*-plots are poorer at plotting space-time events or collisions between flying objects or light beams. Such tasks are done better on Minkowski *(x,ct)* plots.

Fig.11 further connects the TRM of Fig.8 to earlier geometry in Fig.4 thru Fig.6 by drawing together all hyperbolas, circles, and connecting tangents. This includes a clear construction of the stellar aberration ray and the corresponding **k**-vector at stellar angle σ it attains in TE waveguide of Fig.12 where the wavefront **C′SY** is normal to **k**.

Prime phase point **P′** in Fig.11 at $(v, c\kappa)$=B(sinhρ,coshρ) is on Alice's v_A-axis **OP′** of slope cothρ. **P′** is a hyperbolic tangent point for line **LP′R** of slope tanhρ=$\frac{LL'}{RL'}$ with axis intercepts equal to |**QO**|=Bcschρ and |**AO**|=Bsechρ. **P′Q** parallels **G′** line of group $c\kappa_A$-axis. Prime stellar point **S′** at coordinates $(v, c\kappa)$=B(sechρ,tanhρ) defines stellar ray **OSk** of slope cschρ . **S** is b-circle tangent point for line **C′SY** of slope -sinhρ =-$\frac{A'S}{AS}$ with axis intercepts |**C′O**|=Bcoshρ and |**OY**|=Bcothρ. ρ-functions relate to σ-functions in Table I.

Applications that follow use a pattern-recognition aid labeled *Occam's Sword* in Fig.

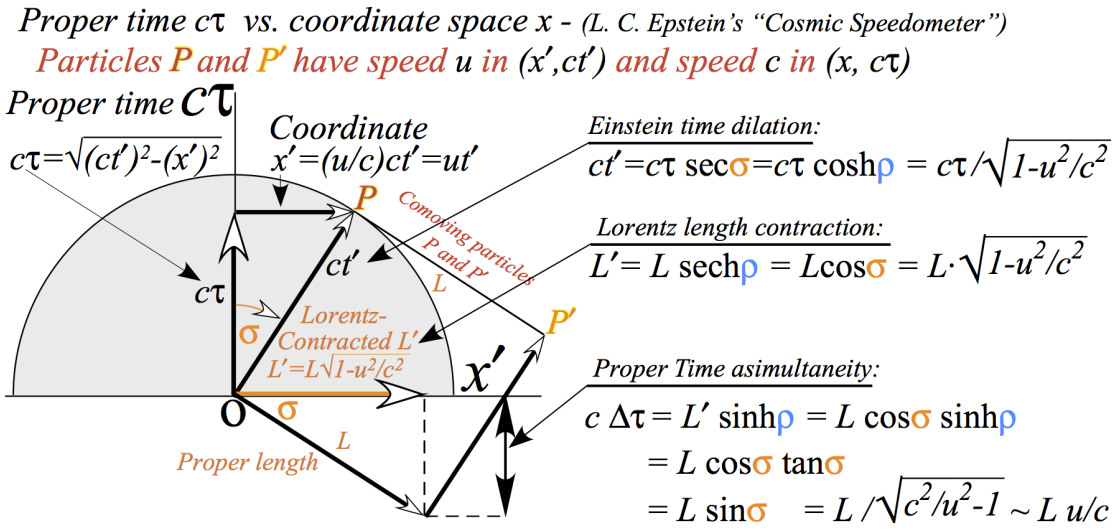

FIG. 10: Epstein space-proper-cτ geometry of relativistic effects in terms of ρ or σ.

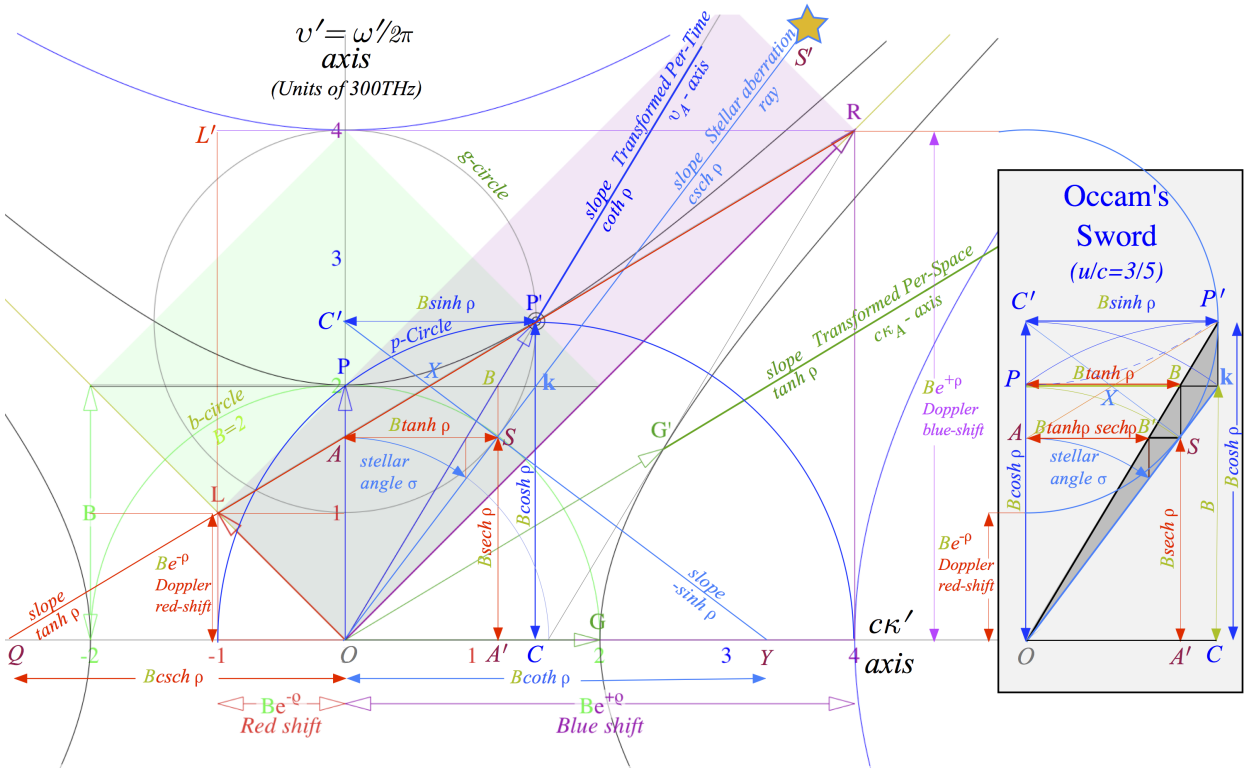

FIG. 11: Bob-(υ',cκ')-view of Alice-(υ_A,cκ_A) tangent geometry and (inset) Occam-Sword pattern relates σ, ρ, and υ angles.

11(inset). It focuses on geometry of (sin⇌tan) and (cos⇌sec) columns of Table I. The (cot⇌csc) intercepts are outliers for low u/c values and lie at $\pm\infty$ for $\rho = 0 = \sigma$.

The sword has staircase steps following a $(\cosh\rho)^n$-geometric series: ($B\cosh\rho$,B,$B\mathrm{sech}\rho$,...). Multiplying series by $\tanh\rho$ gives line ($|\mathrm{C'P'}|{=}B\sinh\rho$), then line($|\mathbf{PB}|{=}B\tanh\rho$), and lowest step ($|\mathbf{AB'}|{=}B\tanh\rho\ \mathrm{sech}\rho$). Steps subtend a triple-cross-X-point of tangents $\mathbf{C'XS}$, $\mathbf{AXP'}$, and b-baseline $\mathbf{PXB}$. Extensions of the tangents have κ-axis (cot⇌csc)-intercepts on either side of the sword in Fig.11. Compare Fig.11 to TRM of Fig. 8. The sword's leading k-edge defines wavevectors for TE-waveguides so them are easier to visualize as shown below.

1. *TE-Waveguide geometry*

Consider a sum of plane waves with wave-vectors $\mathbf{k}(+){=}(k\sin\sigma,{+}k\cos\sigma){=}(kx,ky)$ pointing up in Fig.12a and $\mathbf{k}(\text{-}){=}(k\sin\sigma,\text{-}k\cos\sigma){=}(k_x,k_y)$ pointing down, each an angle $\pm\sigma$ relative to the y-axis in Fig.12.

$$E_z(\mathbf{r},t)\ =\ e^{i(\mathbf{k}^{(+)}\cdot\mathbf{r}-\omega\cdot t)}+e^{i(\mathbf{k}^{(-)}\cdot\mathbf{r}-\omega\cdot t)}\ =\ e^{i(k_x\cdot x-\omega\cdot t)}[e^{ik_y\cdot y}+e^{-ik_y\cdot y}] \tag{15}$$

The result in xy-plane is a Transverse-Electric-(TE)-mode $\mathbf{E}$-field with plane-normal z-component Ez that vanishes on metallic floor and ceiling (y=±Y/2) of the waveguide.

$$E_z(\mathbf{r},t)=e^{i(k\cdot x\sin\sigma-\omega\cdot t)}2\cos(ky\cos\sigma)|_{y=\frac{Y}{2}}\ =\ 0\quad\text{implies}:\quad k\frac{Y}{2}\cos\sigma=n\frac{\pi}{2} \tag{16}$$

Fig.12 shows two cases of lowest ($n{=}1$) guide modes with *Occam-sword* geometry. Projection $Y\cos\sigma$ of floor-to-ceiling Y onto $\mathbf{k}(\pm)$-vectors is shown by right triangles at guide ends (16) to be half-wave $\frac{\pi}{k}=\frac{\lambda}{2}$. Waveguide angle σ and dispersion function $\upsilon(\kappa)$ follows.

$$\upsilon\ =\ c\kappa\ =\ c\sqrt{\kappa_x^2+\kappa_y^2}=c\sqrt{\kappa_x^2+\kappa^2\cos^2\sigma}=\sqrt{c^2\kappa_x^2+(\frac{c}{2Y})^2}\ =\ \sqrt{c^2\kappa_x^2+\upsilon_A^2} \tag{17}$$

Surprising insight into Fig.12 waves results if we note it is what Bob sees if Alice and Carla point their υ_A = 600THz 2-CW beam *across* Bob's x-line of motion at angle σ to y and not *along* x as in Fig. 4b. Bob can Doppler shift his wave-number κ_xx and angle σ to zero and reduce frequency υ in (17) to $\upsilon=\upsilon_A$. Then Bob will be co-moving with Alice and Carla and see Alice's $\mathbf{k}(+)$-vector at zero aberration angle ($\sigma=0$) if she is below Fig.12 beaming straight up the y-axis. Meanwhile, Carla's $\mathbf{k}$(-)-vector points straight down. For ($\sigma=0$) the wave given by (16) is a y-standing wave of wavelength $\lambda_A{=}2Y$ between Alice and Carla, not just a half-wave section ($Y{=}\frac{\lambda}{2}$) of a lowest mode of this xy-wave guide.

Ideally Alice and Carla's laser mode viewed along y looks like their x-standing wave in Fig.4b or Fig.5b and appears the same over its x-beam-width by having zero x-wave number

($\kappa_x = \kappa_A sin\sigma = 0$). Zero-$\kappa_x$ or infinite x-wavelength ($\lambda_x = \lambda_A csc\sigma = \infty$) is a flat-line wave parallel to the x-axis oscillating at Alice's (or Carla's) 600THz frequency υ_A.

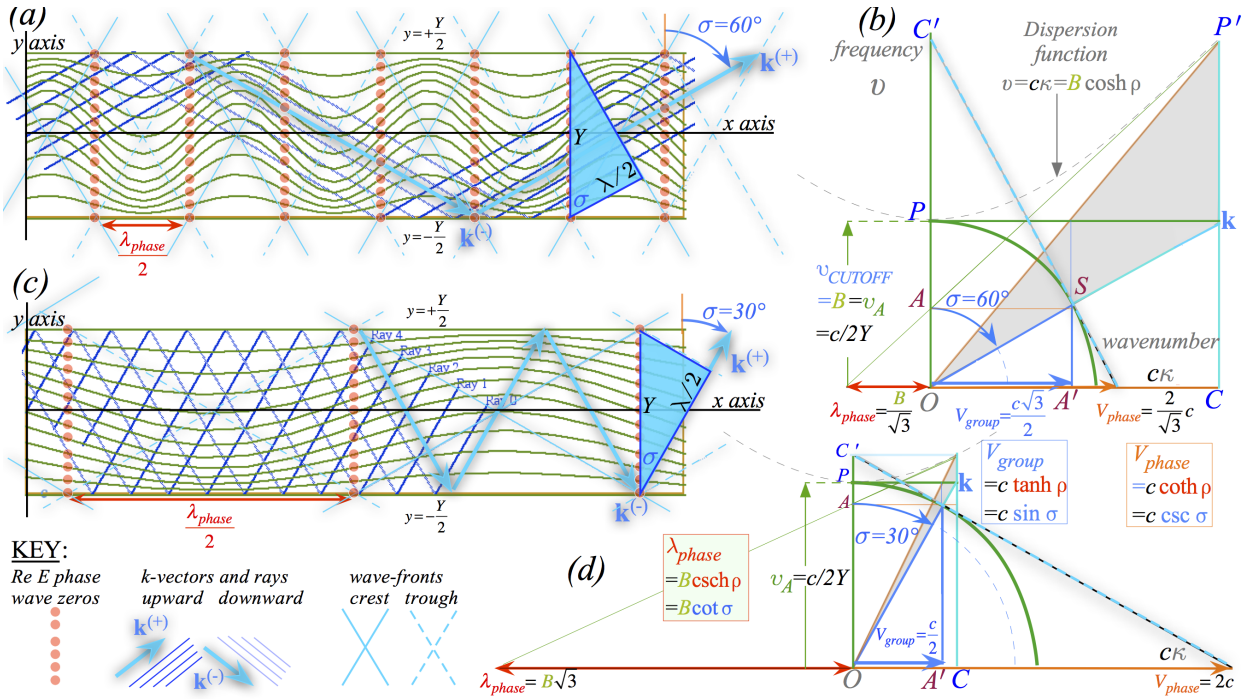

FIG. 12: TE-Waveguide and Occam sword angle (a-b) $\sigma = 60°$ and (c-d) $\sigma = 30°$.

This x-flat wave is better known in wave guide theory as a *cut-off-frequency* mode where the cut-off-frequency $\upsilon_{CUTOFF} = \frac{c}{2Y} = \upsilon_A$ is the lower bound to frequency that can enter a waveguide of width Y. In Fig. 12b it corresponds to dispersion function bottom point **B** (or **P**) that is well separated from its phase point $\mathbf{P}'$ in the upper right of the figure. That separation $|\mathbf{OC}|$=Bsinhρ =Btanσ gives a mode in Fig.12a that is more robust than the near-cutoff mode in Fig.12c having less $|\mathbf{OC}|$ and a more nearly vertical $\boldsymbol{k}$-vector in Fig. 12c-d. The tanσ-column of Table I represents the phase wave-number ratio κ_{phase} /κ_A of Bob's κ_{phase} to κ_A that Alice and Carla claim is their output. Later it is shown that $|\mathbf{OC}|$ = κ_x is mode wave momentum while vertical interval $|\mathbf{CP'}|$=Bcoshρ =B secσ = υphase or phase frequency ratio $\upsilon_{phase}/\upsilon_A$ in Table I correspond to mode carrier wave energy. These determine wave robustness and phase velocity V_{phase}/c is equal to their ratio $\upsilon_{phase}/\kappa_{phase}$ = $\lambda_{phase}/\tau_{phase}$. The importance of waveguide phase or carrier behavior is matched by that of group or signal wave dynamics. Each has six of twelve variables listed in Table I. Matching phase velocity V_{phase}/c = cothρ = cscσ is reciprocal to V_{group}/c = tanhρ = sinσ.

Both are indicated by arrow lengths at the base of Occam Sword plots in Fig. 12b or Fig.12d. The latter has V_{group} much lower than V_{phase} while the former has both closing in on light speed c. Group velocity V_{group} equals projection $c\sin\sigma$ of $c\hat{\mathbf{k}}$-vector onto the waveguide x-axis. One may imagine a signal bouncing off guide floor or ceiling riding on the $\mathbf{k}$-vectors normal to phase wavefronts moving at speed c along $\mathbf{k}(+)$ or $\mathbf{k}(-)$ in Fig.12a or Fig.12c. So a signal wastes time bouncing around the guide x-axis while the phase crests proceed via a greater speed $c\ \csc\sigma$. A signal may be imagined as an extra wrinkle in symmetry of identical wave crests due to lately added Fourier components limited by envelope group velocity. Meanwhile an established underlying phase maintains Evenson's c-lock-step. Per-space-time $(v,c\kappa_x)$ geometry of Fig.12b or Fig.12d rules that of space-space (x,y) in Fig.12a or Fig.12c.

E. Unbalanced optical amplitudes

What has been deduced so far has ignored the *amplitude* or *quantity* of light waves and concentrated mostly on their *quality* as described by *phase* parameters such as angular frequency ω and wave vector k. The Evenson 1-CW phase axiom (*All colors go* c.) leads to Bob *vs* Alice-Carla transformation (7a) and (7b) while 2-CW amplitudes in (5) are not defined beyond assuming that head-on 1-CW component amplitudes match. White-line standing wave grid reference frames in Fig.1b and Fig.4b are just points where amplitudes are zero, that is, loci of real wave function *roots*.

Discussion of asymmetric amplitudes begins with counter-propagating 2-CW dynamics of two 1-CW amplitudes A_R and A_L that may be *un*matched. $(A_R \neq A_L)$

$$A_R e^{i(k_R x-\omega_R t)}+A_L e^{i(k_L x-\omega_L t)} = e^{i(k_\Sigma x-\omega_\Sigma t)}[A_R e^{i(k_\Delta x-\omega_\Delta t)}+A_L e^{-i(k_\Delta x-\omega_\Delta t)}] \tag{18}$$

This uses half-sum(or half-difference) k-vector k_Σ (or k_Δ) and frequency ω_Σ (or ω_Δ).

$$k_\Sigma{=}\ (k_R+k_L)/2, \quad k_\Delta{=}\ (k_R{-}\ k_L)/2, \quad \omega_\Sigma{=}\ (\omega_R+\omega_L)/2, \quad \omega_\Delta{=}\ (\omega_R{-}\ \omega_L)/2.$$

Ratio of $\frac{1}{2}$-sum $A_\Sigma{=}(A_R+A_L)/2$ and $\frac{1}{2}$-difference $A_\Delta{=}(A_R-A_L)/2$ is *Standing-Wave-Ratio* SWR or (inverse) *Standing-Wave-Quotient* SWQ that relate to real-wave velocity.

$$\text{SWR} = \frac{A_R-A_L}{A_R+A_L}, \qquad \text{SWQ} = \frac{A_R+A_L}{A_R-A_L}. \tag{19}$$

Frequency ratio (11) defining group velocity V_{group} is analogous to SWR and V_{phase} to SWQ.

$$V_{group} = c\frac{\omega_\Delta}{k_\Delta} = c\frac{\omega_R - \omega_L}{\omega_R + \omega_L}, \qquad V_{phase} = c\frac{\omega_\Sigma}{k_\Sigma} = c\frac{\omega_R + \omega_L}{\omega_R - \omega_L}. \tag{20}$$

A 2-state amplitude continuum is bounded by a pure right-moving 1-CW (A_R =1, A_L =0) of SWR=1 and a left-moving 1-CW (A_R = 0, A_L =1) of SWR=-1. Midway between is the normalized 2-CW standing-wave having SWR=0.(A_R=$\frac{1}{\sqrt{2}}$=A_L) Wave paths for other SWR values are drawn in Fig.13.1a-e for 600THz 2-CW pairs and in Fig.13.2a-e for Doppler shifted 300THz and 1200THz 2-CW pairs at the same SWR values. The SWQ is the ratio of the envelope peak (interference maximum) to the envelope valley (interference minimum), and vice versa for SWR=1/SWQ.

1. *Wave galloping speed bounded by SWR*

Single frequency 2-CW paths of nonzero-SWR in Fig.13.1 do a galloping motion (derived below) while dichromatic 2-CW in Fig.13.2d-e have zero paths that follow Feynman-Wheeler time switchbacks. Waves in Fig.13.1b speed up to a peak speed of c/SWR=5c as it shrinks to squeeze through its envelope minima and then slows to minimum speed cSWR=c/5 as it expands to its maximum amplitude. Only at zero-SWR do 2-CW zero-paths appear to travel at a constant group speed (20a) and phase speed (20b) as in Fig.13.1c and in Fig.13.2c. For SWR=1 or SWR=-1 there is just a single wave and one speed $\pm c$ following Evenson's axiom. Real and imaginary parts take turns. One gallops while the other rests and this occurs twice each optical period.

Galloping is a fundamental interference property that may be clarified by analogy with elliptic orbits of isotropic 2D-harmonic oscillators and in particular with elliptic polarization of optical wave amplitudes. Fig.14 relates polarization states to wave states of Fig.13.1 beginning with left (right)-circular polarization that is analogous to a left (right)-moving wave in Fig.14g (Fig.14a). As sketched in Fig.14(b-e), galloping waves are general cases analogous to states of elliptic polarization or general 2D-HO orbits obeying a Keplerian geometry shown in Fig.14h. Standing waves correspond to plane-polarization. Polarization in x-plane of Fig.14d corresponds to a standing cosine wave. y-plane polarization (not shown) corresponds to a standing sine wave.

Isotropic oscillator orbits obey Kepler's law of constant orbital momentum. Orbit angular

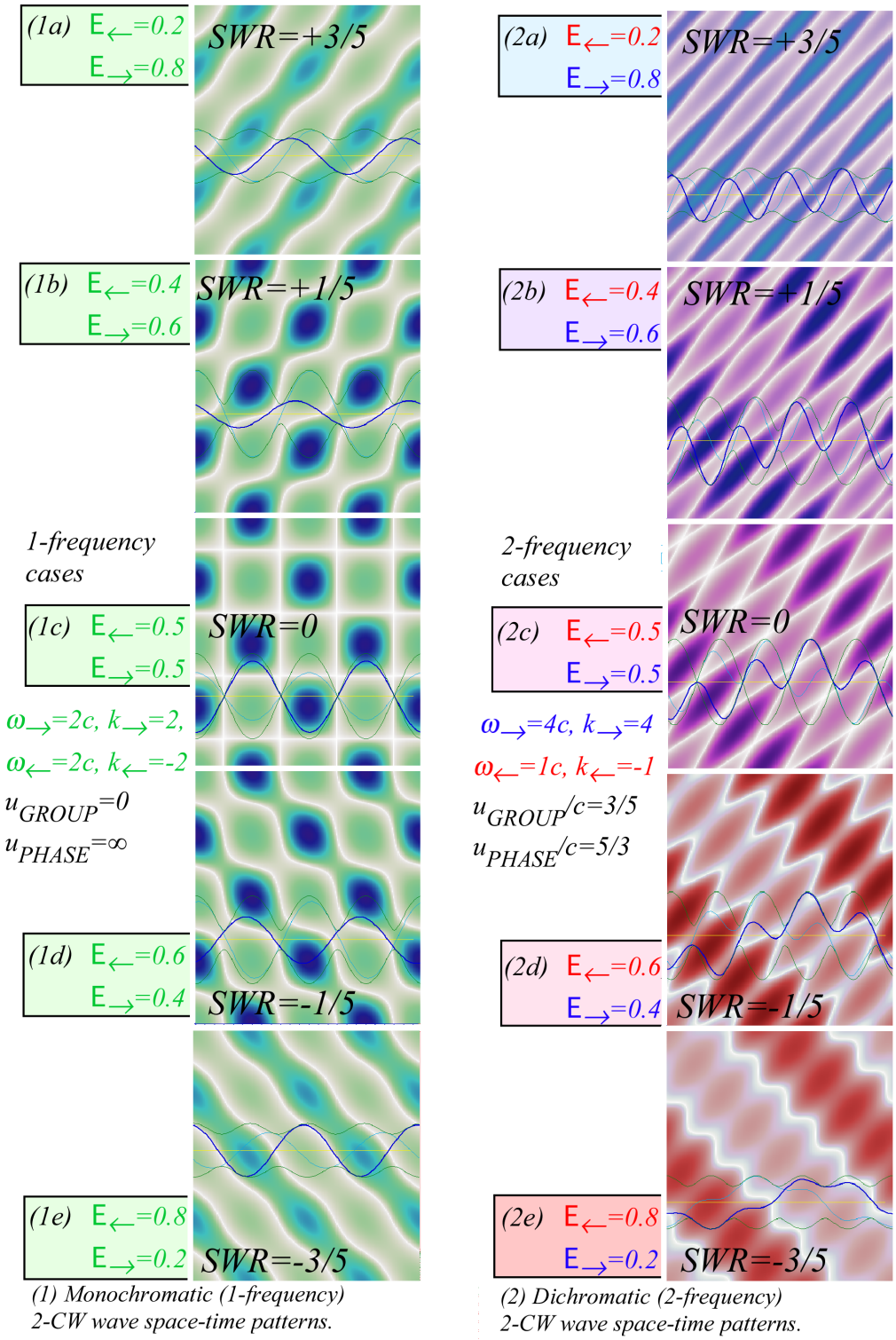

FIG. 13: 2-CW (x,ct)-paths for $\frac{-3}{5} \leqslant \text{SWR} \leqslant \frac{3}{5}$ (1a-e) Single-frequency (2a-e) 2-frequency.

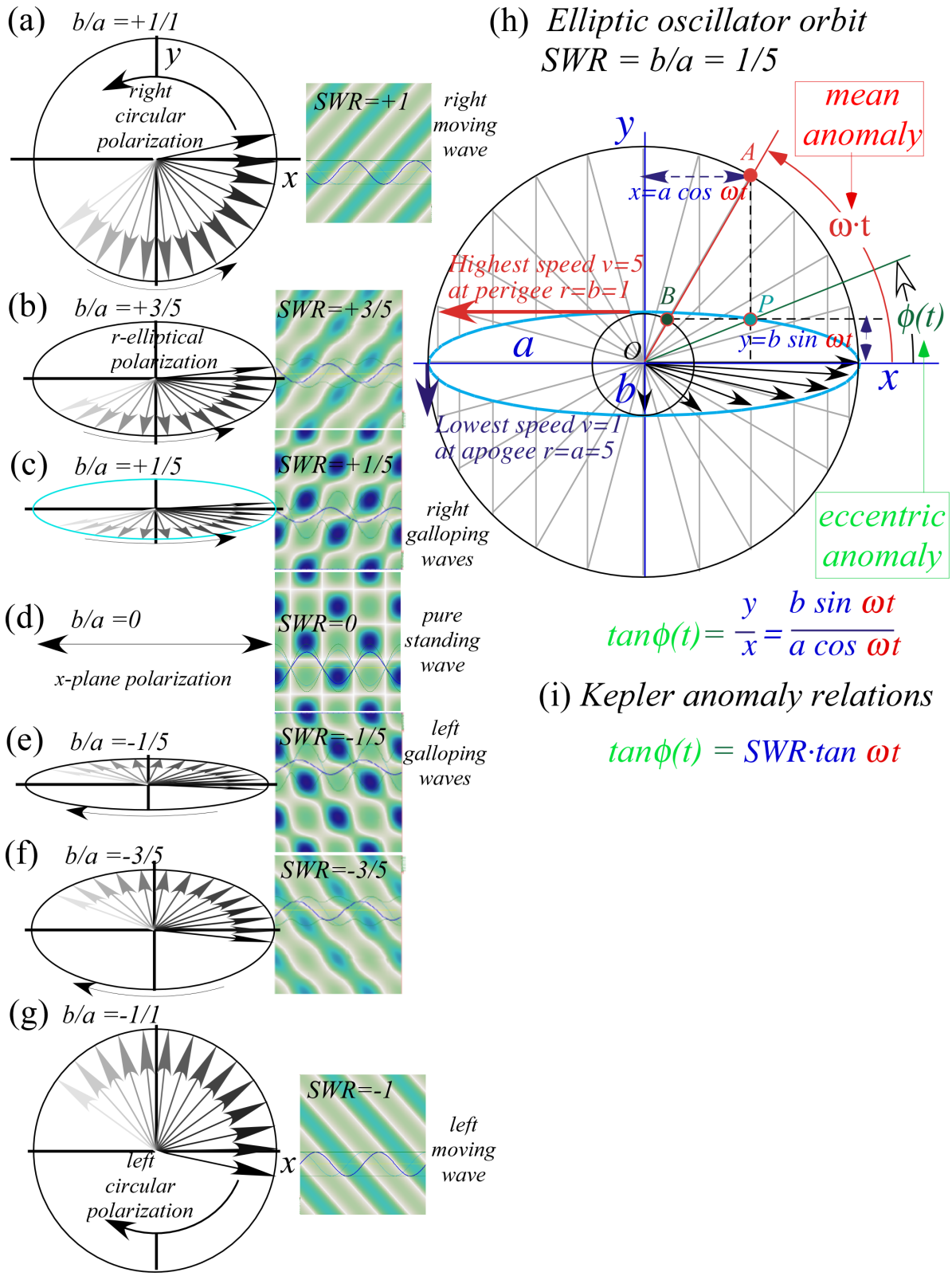

FIG. 14: 2-CW (x,ct)-paths for $\frac{-3}{5} \leqslant \text{SWR} \leqslant \frac{3}{5}$ (1a-e) Single-frequency (2a-e) 2-frequency.

velocity slows down by a factor b/a at the aphelion a and then speeds up by a factor a/b at the perihelion b just as a galloping wave, twice in each period, slows down to SWR$\,c$ and speeds up to SWQc. Galloping motion of the eccentric anomaly angle $\phi(t)$ in Fig.14h is a projection of a uniformly rotating mean anomaly (phase angle ωt) of the isotropic oscillator that relates these two angles.

$$\tan\phi(t) = \frac{b}{a}\tan(\omega t) \tag{21}$$

Eccentric anomaly t-derivative gallops between $\omega\frac{b}{a}$ and $\omega\frac{a}{b}$.

$$\dot{\phi} = \frac{d\phi}{dt} = \omega\frac{b}{a}\frac{\sec^2\omega\, t}{\sec^2\phi} = \frac{\omega\frac{b}{a}}{\cos^2\omega\, t + \left(\frac{b}{a}\right)^2\cdot\sin^2\omega\, t} = \begin{cases} \omega\frac{b}{a} \text{ for:} \omega\, t = 0, \pi, 2\pi... \\ \omega\frac{a}{b} \text{ for:} \omega\, t = \pi/2, 3\pi/2, ... \end{cases} \tag{22}$$

Angular moment r^2 times $\dot{\phi}$ is proportional to orbital momentum and orbit ellipse area πab.

$$r^2\frac{d\phi}{dt} = constant = (a^2\cos^2\omega\, t + b^2\cdot\sin^2\omega\, t)\frac{d\phi}{dt} = \omega\cdot ab \tag{23}$$

A monochromatic ($\omega_R = \omega_0 = \omega_L$) wave (18) can gallop like (22) with SWQ=$\frac{a}{b}$>1 in (19).

$$0 = \mathrm{Re}\Psi\,(x,t) = \mathrm{Re}A_R e^{i(k_0x-\omega_0t)} + \mathrm{Re}A_L e^{i(-k_0x-\omega_0t)} \quad \text{where: } \omega_R{=}\omega_0{=}\,\omega_L \,{=}ck_R{=}{-}ck_L$$

This real-zero relation factors: $(A_{\rightarrow}{+}A_{\leftarrow})[\cos k_0x\ \cos\omega_0t]{=}-\,(A_{\rightarrow}{-}A_{\leftarrow})[\sin k_0x\ \sin\omega_0t]$. So space k_0x varies with time ω_0t quite like eccentric anomaly $\phi(t)$ varies in (21) or (22).

$$\tan k_0x = -SWQ\cdot\cot\omega_0t = SWQ\cdot\tan\omega_0\bar{t} \quad \text{where}: \ \omega_0\bar{t} = \omega_0t - \pi/2$$

$$\frac{dx}{dt} = c{\cdot}SWQ\frac{\sec^2\omega_0\bar{t}}{\sec^2k_0x} = \frac{c{\cdot}SWQ}{\cos^2\omega_0\bar{t} + SWQ^2{\cdot}\sin^2\omega_0\bar{t}} = \begin{cases} c{\cdot}SWQ \text{ for: } \bar{t} = 0, \pi, 2\pi... \\ c{\cdot}SWR \text{ for: } \bar{t} = \frac{\pi}{2}, \frac{3\pi}{2}, ... \end{cases} \tag{24}$$

Single frequency 2-CW paths in Fig.13.1 have a constant product (23) of wave velocity and wave amplitude analogous to constant product of orbital velocity and radius. Dichromatic paths in Fig.13.2 are analogous to aniostropic 2D oscillators with varying (23). Fig.13.2d wave-zero paths follow Feynman-Wheeler time switchbacks where pairs of zeros with slopes of opposite sign are created then annihilated later by neighboring zeros. So optical amplitude and phase motion obey strange versions of 14th century Keplerian geometry rules. It may surprise some the extent to which such ancient rules underlie basic wave physics and quantum wave dynamics that are described next.

IV. RELAWAVITY GIVES QUANTUM MECHANICS OF MATTER

Since the last century, fundamental developments of quantum mechanics have relied on concepts from advanced classical mechanics of Lagrange, Hamilton, Legendre, Jacobi, and Poincare that were developed mostly in the preceding(19^{th}) century. The latter contain a formidable web of formalism using ecclesiastical terms such as *canonical* that once implied higher levels of truthiness, but for modern physics students, they mean not so much.

Below is a simpler approach that connects wave geometry of Sec. II B to 16^{th} through 18^{th} century mechanics of Galileo, Kepler, and Newton and then derives mechanics fundamentals for the 20^{th} and 21^{st} centuries. It also clarifies some 19^{th} century concepts that are often explained poorly or not at all. This includes Legendre contact transformations, canonical momentum, Poincare invariant action, and Hamilton-Jacobi equations. Understanding of these difficult classical ideas and connections is helped by the geometry of *relawavity*.

2-CW geometry of Fig. 11 has hyperbolic coordinates of phase frequency υ_{phase}=$B cosh\rho$ and c-scaled wave number $c\kappa_{phase}$ =$B sinh\rho$ with slope equal to group velocity V_{group}/c = $u/c = tanh\rho$. Each depends on rapidity ρ that approaches u/c for Newtonian speeds $u \ll c$.

$$\begin{aligned} \upsilon_{phase} &= B\cosh\rho \approx B + \tfrac{1}{2}B\rho^2 \quad (\text{for } u \ll c) \\ c\kappa_{phase} &= B\sinh\rho \approx B\rho \quad (\text{for } u \ll c) \\ u/c &= \tanh\rho \approx \rho \quad (\text{for } u \ll c) \end{aligned} \tag{25}$$

At these low speeds κ_{phase} and υ_{phase} are functions of group velocity u=$c\rho$ or u^2=$c^2\rho^2$. The hyperbolic base coefficient B has frequency units (1Hz =$1s^{-1}$) of υ_{phase} and cκ_{phase} so the same scale factor B/c^2 multiplies both u^2 and u.

$$\upsilon_{phase} \approx B + \tfrac{1}{2}[B/c^2]u^2 \qquad \Leftarrow \text{for}(u \ll c) \Rightarrow \qquad \kappa_{phase} \approx [B/c^2]\,u \tag{26}$$

From freshman physics is recalled kinetic energy KE=$const.$+$\frac{1}{2}Mu^2$ and Galilean momentum p=Mu. One *Joule·s* scale factor h=Mc^2/B gives υ_{phase} energy units and κ_{phase} momentum units. Then these wave coordinates give classical KE and p formulas. But, an annoying (and large) constant Mc^2 is added to KE!

$$h\upsilon_{phase} \approx Mc^2 + \frac{1}{2}Mu^2 \qquad \Leftarrow \text{for}(u \ll c) \Rightarrow \qquad h\kappa_{phase} \approx M\,u \tag{27}$$

One may ask, "Is this just a lucky coincidence?"

The answer involves the base or bottom value $B{=}v_A$ of Alice's frequency hyperbola. It is also Bob's bottom due to hyperbola invariance. The constant $const.{=}hB{=}hv_A{=}Mc^2$ may be the most famous formula in physics. Here it is Einstein's rest-mass-energy equation. It is an add-on to Newton's kinetic energy $\frac{1}{2}Mu^2$ that is perhaps the *second* most famous physics formula. This add-on does not contradict Newton's result. Physical effects depend only on difference or change of energy so effects of an add-on vanish. The question of false coincidence criticizes (27) for Galilean-Newtonian formulas is valid only at low velocity ($u{\ll}c$) or low ρ. So approximate v_{phase} and κ_{phase} in (27) need to be replaced by Table I formulas $v_{phase}{=}B\cosh\rho$ and $c\kappa_{phase}{=}B\sinh\rho$ that hold for *all* ρ.

$$\begin{aligned} E = hv_{phase} = Mc^2\cosh\rho \qquad &\Leftarrow \text{for } all\ \rho \Rightarrow \qquad p = h\kappa_{phase} = Mc\sinh\rho \\ = \tfrac{Mc^2}{\sqrt{1-u^2/c^2}} \qquad &\Leftarrow \text{for } |u|<c \Rightarrow \qquad = \tfrac{Mu}{\sqrt{1-u^2/c^2}} \end{aligned} \tag{28}$$

The old-fashioned $\beta{=}u/c$ form of $\cosh\rho$ (Table I) is Einstein[2] 1905 total energy formula. Later in 1923, DeBroglie gives wave momentum formula[3] $p = \hbar k = h\kappa$ that has a $\beta{=}u/c$ form for $\sinh\rho$, too. Three lines above derive both ρ-forms in (28) from Table I. This allows physics students to enjoy one-button-press calculator-recall as well as the geometric and algebraic elegance of relawavity insight discussed below.

Underlying (28) is considerable physics and mystery of "scale factor" h (or $\hbar \equiv h/2\pi$) the Planck constant $h{=}6.62607{\cdot}10^{-34}$ Joule·sec that appears in his cavity energy axiom $E_N{=}hNv$. Thus (28) gives just the lowest quantum level ($N{=}1$) of Planck's axiom[4]. (Modern form $E_N{=}\hbar N\omega$ has angular frequency $\omega{=}2\pi v$ and angular $\hbar{=}1.0510^{-34}J{\cdot}s$.) A quick-fix replaces h with hN, but underlying quantum oscillator theory of electromagnetic cavity waves is needed.

So far, the axioms needed for SR results (28) are Evenson's (*All colors go c!*) and time reversal symmetry following Fig.2 and Fig.3. These involve space, time, frequency and phase factors of plane light waves that are sufficient to develop the special relativity theory. But this phase approach has so far ignored amplitude factor A of light wave $\psi = Ae^{i(\mathbf{k}\cdot\mathbf{r}-\omega t)}$. While phase factor $e^{i(\mathbf{k}\cdot\mathbf{r}-\omega t)}$ describes *quality* aspects of the light, an amplitude factor A describes the *quantity* of light, or more to the point, an average number N of *quanta* or *photons* in a wave having the N factor of Planck's axiom. Raising N raises overall phase frequency Nv_{phase} and in proportion, both total energy hNv_{phase} and total wave *quantum-mass* $M_N = (hNv_{phase})/c^2$. (As seen below, this "light's weight" is tiny unless N is *astronomical*.)

The logical efficiency of optical axioms leading to (28) sheds some light on the three of the most logically opaque concepts of physics, namely energy, momentum and mass by expressing them as phase frequency υ (inverse time τ) and wavenumber κ (inverse length λ). Perhaps, the terms *energy* and *momentum* could someday go the way of *phlogiston*[5]!

A. What is energy?

A student asks a professor lecturing on energy, "What is *Energy*?" The prof. replies, "It measures ability to do *Work*." The student persists:"What is *Work*?" The reply: "Well, it's *Energy*, of course!"

The Prof. might well give the same circular logic if asked about *momentum*, another *sine qua non* of basic physics. A favorite flippant response to E and p questions is that momentum is the *"Bang"* and energy is the $\$Buck\$$ that pays for it. (*$1.00=10kWHr* is close to national average.) This belongs to an (unfortunate) U.S expression "Get more bang for your buck!" Perhaps, but only on the 4^{th} of July.

Wave energy and momentum results (28) defeat such circular logic by showing how energy E is proportional to temporal frequency (υ_{phase} waves per second) and momentum p_α is proportional spatial frequency (κ_{phase} waves per meter in direction α). One should note the ratio of momentum p and energy E in (50) is $\frac{c\mathbf{p}}{E} = \frac{c\mathbf{k}}{\omega} = \frac{\mathbf{u}}{c}$. It is a correct wave velocity relation for any scale-factor h (or hN).

The answer in (28) for wave energy inside Alice's laser cavity is a product of her quantum tick-rate $\upsilon_{phase}= \upsilon_A = 600\text{THz}$, scale factor h (actually hN), and Einstein dilation factor $\cosh\rho$ that is $\cosh 0=1$ for her and $\cosh\rho = \frac{5}{4}$ for Bob in Fig.4b. Bob might complain about her $\frac{4}{5}$-shortened wavelength $\lambda_{group} = (\frac{1}{2}\mu m)sech\rho = \frac{1}{2}\frac{4}{5}\mu m$ instead of complimenting her for $\frac{5}{4}$ more wave energy. (When you can't say something nice...) Bob may not see her considerable increase of momentum from zero ($\sinh 0=0$) to

$$p = hN\kappa_{phase} = hN\kappa_A \sinh\rho = hN\tfrac{\upsilon_A}{c}\tfrac{3}{4}.$$

He is excused for overlooking such a tiny momentum. (p has a $\frac{1}{c}$-factor that is not in E.)

$$E = hN\upsilon_A \cosh\rho = hN\upsilon_A\tfrac{5}{4}$$

A most remarkable thing about (energy, momentum)$\propto$ $(\upsilon_{phase}, \kappa_{phase})$ relations (28) (now with hN in for h) and the Alice-Bob story is that (28) applies not just to Alice's light

wave but also to its laser cavity frame. (Recall discussion after (10).) In fact *any* mass M (including Alice and Bob themselves) is made of waves with an internal "heartbeat" frequency $\upsilon_{phase} = Mc^2/Nh$ that is *incredibly* fast due to the c^2-factor and tiny Planck-h divisor. Also, Alice's light wave with $\upsilon_{phase}= \upsilon_A$ has a mass $M_A = Nh\upsilon_A/c^2$ that is *incredibly* tiny here due to *both* a tiny Planck-h factor and enormous c^2-divisor.

1. *What's the matter with energy?*

Evenson axioms of optical dispersion and time symmetry imply a 2-CW light geometry that leads directly to exact mass-energy-momentum and frequency relations (28) with low-speed approximations (27). A light wave with rest mass and rest energy proportional to a proper invariant phase frequency

$$\upsilon_{phase} = \upsilon_A = \upsilon'_A$$

is effectively a quantum matter wave that, due to its $N\upsilon_{phase}$=$N\upsilon_A$, has intrinsic rest mass.

$$M_{A_N} = Nh\upsilon_A/c^2$$

In so doing, concepts of mass or matter lose classical permanence and become fungible. We define three types of mass M_{rest}, M_{mom} *and* M_{eff} distinguished by their dependence on rapidity ρ or velocity u. The first is $M_{rest} = M_{A_N}$, a constant. The other two approach M_{rest} at low u≪c.

Einstein rest mass M_{A_N} is invariant to ρ. It labels a hyperbola with a bottom base level B.

$$E_N(\rho = 0) = hB = M_{A_N}c^2$$

This label is respected by all observers including Alice and Bob. Each mode A of Alice's cavity has a stack of N=1,2,3,... hyperbolas, one for each quantum number N-value.

$$\begin{aligned} E_N^2 &= (hN\upsilon_A)^2 = (M_{A_N}c^2)^2\cosh^2\rho = (M_{A_N}c^2)^2(1+\sinh^2\rho) \\ &= (M_{A_N}c^2)^2 + (cp_N)^2 \end{aligned} \tag{29}$$

(E,cp)-space hyperbola $E = \sqrt{(Mc^2)^2 + (cp)^2}$ in Fig.15 is a plot of an exact Einstein-Planck matter wave dispersion (28). The inset is a plot of approximation (27) for low p and $u \ll c$. Properties and pitfalls of this *Bohr*[6]*-Schrodinger*[7] *approximation* are discussed later.

The second type of mass M_{mom} is *momentum-mass* defined by ratio p/u of relativistic momentum $p{=}Mc\ sinh\rho$ from (28) with group velocity $u{=}c\ \tanh\rho$. M_{mom} follows the old Galileian quasi-definition $p{=}M_{mom}u$ with newly defined relativistic wave group velocity $u = c\tanh\rho$ substituted from (9a).

$$\begin{aligned} &\tfrac{p}{u} \equiv M_{mom} = \tfrac{M_{rest}c}{u}\sinh\rho = M_{rest}\cosh\rho \xrightarrow[u\to c]{} M_{rest}e^{\rho}/2 \\ &= \tfrac{M_{rest}}{\sqrt{1-u^2/c^2}} \xrightarrow[u\ll c]{} M_{rest} \end{aligned} \tag{30}$$

A third type of mass M_{eff} is effective-mass defined by ratio dp/du of *change* of momentum $p{=}Mc\sinh\rho$ from (28) with *change* of group velocity $du = c\,\mathrm{sech}^2\rho d\rho$. M_{eff} satisfies Newton's quite old definition $F{=}M_{eff}a$, but now using relativistic wave quantities.

$$\frac{F}{a} \equiv M_{eff} \equiv \frac{dp}{du} = \frac{dp}{d\rho}\Big/\frac{d\rho}{du} = M_{rest}c\cosh\rho/c\,\mathrm{sech}^2\rho = M_{rest}\cosh^3\rho \tag{31}$$

Another derivation of M_{eff} uses group velocity $V_{group} = \frac{dv}{d\kappa} = u$ as the independent variable.

$$\begin{aligned} &\tfrac{F}{a} \equiv M_{eff} \equiv \tfrac{dp}{du} = \tfrac{hd\kappa}{dV_{group}} = h\Big/\tfrac{d}{d\kappa}\tfrac{dv}{d\kappa} = h\Big/\tfrac{d^2v}{d\kappa^2} \\ &= M_{rest}\Big/(1-u^2/c^2)^{3/2} \xrightarrow[u\ll c]{} M_{rest} \end{aligned} \tag{32}$$

Group velocity and its tangent geometry is a crucial but hidden part of the matter wave theory. Physicists tend to commit to memory a derivative formula $\frac{dv}{d\kappa} = \frac{d\omega}{dk}$ for group velocity and forget $\frac{\Delta v}{\Delta\kappa} = \frac{\Delta\omega}{\Delta k}$ that is a finite-difference formula from which the former is derived. $\frac{dv}{d\kappa}$ may give wrong results since $\frac{\Delta v}{\Delta\kappa}$ is *exact* for discrete frequency spectra while $\frac{dv}{d\kappa}$ may be ill-defined. The wave Minkowski coordinate geometry starts with half-difference ratios to give V'_{group} in primary u-formulae (8) and (9).

$$V'_{group}/c = \frac{\Delta v}{c\Delta\kappa} = \frac{v_R - v_L}{v_R + v_L} = \frac{e^{\rho} - e^{-\rho}}{e^{\rho} + e^{-\rho}} = \tanh\rho \tag{33}$$

What follows in Fig.4 through Fig.5 and Fig.11 is based entirely upon the more reliable finite-difference definition $\frac{\Delta v}{\Delta\kappa} = \frac{\Delta\omega}{\Delta k}$ that gives exactly the desired slope.

Nevertheless, Nature is kind to derivative definition $\frac{dv}{d\kappa} = \frac{d\omega}{dk}$ as seen in Fig.11. There hyperbolic tangent slope of line **RL** with altitude $\Delta v = v_R - v_L$ and base $\Delta\boldsymbol{\kappa} = \boldsymbol{\kappa}_R - \boldsymbol{\kappa}_L$ has a finite-difference slope exactly equal to the derivative of the hyperbola at tangent point $\mathbf{P'}$ on phase velocity line $\mathbf{OP'}$. Geometry of Doppler action (33) is at play. That slope

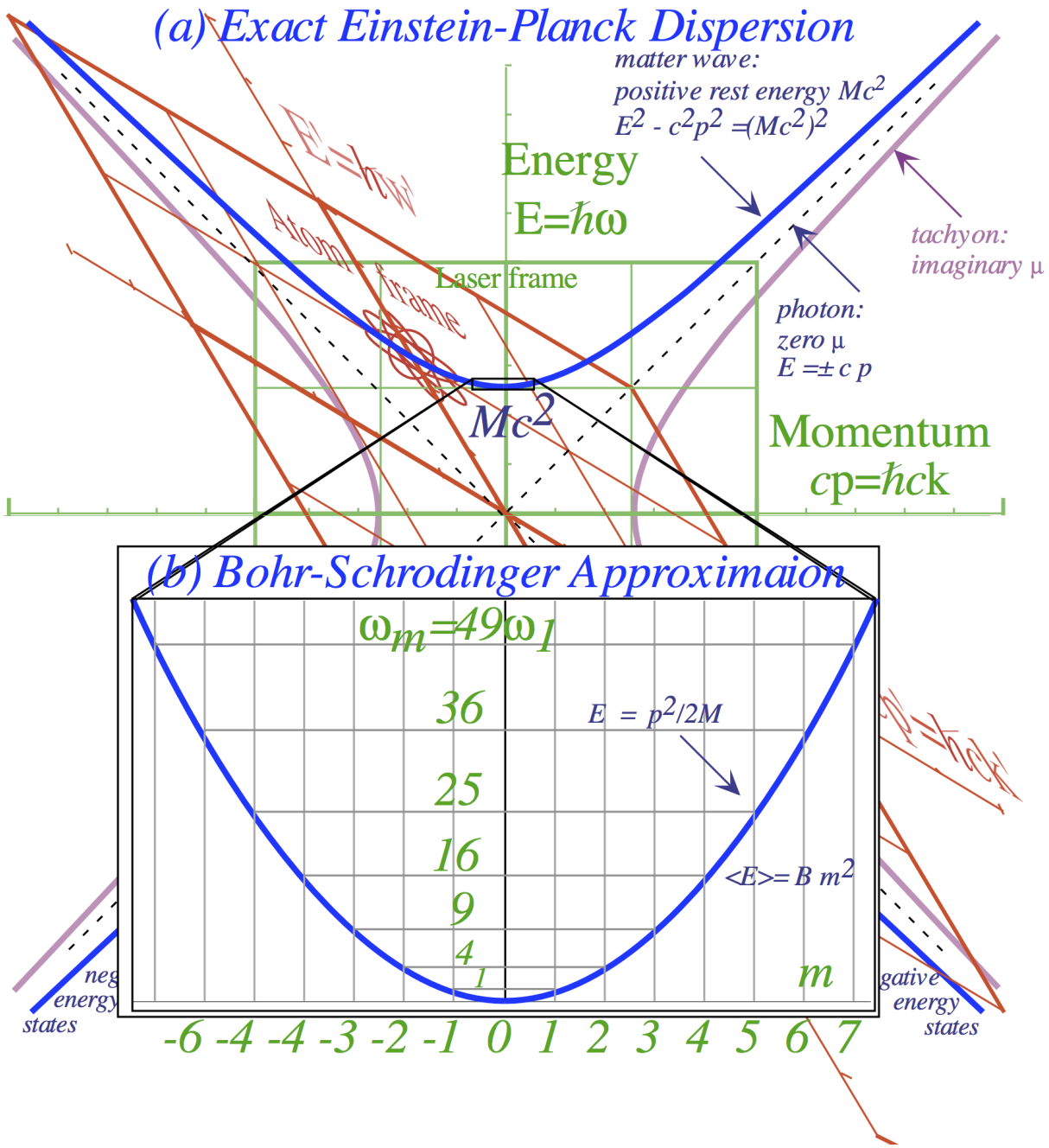

FIG. 15: (a) Einstein-Planck energy-momentum dispersion (b) Bohr-Schrodinger approximation

$\frac{dv}{d\kappa} = \frac{d\omega}{dk}$ equals $V'_{group} = u$ and is the velocity of Alice relative to Bob. It is also related to the momentum/energy ratio $\frac{c\mathbf{p}}{E} = \frac{c\mathbf{k}}{\omega} = \frac{\mathbf{u}}{c}$ noted before.

$$V_{group} = u = \frac{\Delta v}{\Delta \kappa} = \frac{dv}{d\kappa} = \frac{d\omega}{dk} = \frac{dE}{dp} = \frac{c^2 p}{E} \tag{34}$$

As slope $\frac{d\upsilon}{d\kappa} = u$ of dispersion hyperbola $\upsilon(\kappa)$ affects velocity u and relations with momentum p, so does curvature affect acceleration a and its relation to force F or momentum time rate of change $\frac{dp}{dt}$ in the effective-mass M_{eff} equations (31) and (32). One is inclined to regard M_{eff} as a quantum mechanical result since it is a product of Planck constant h with inverse $\frac{d^2\upsilon}{d\kappa^2}$, the approximate *Radius of Curvature* $RoC{=}1/\frac{d^2\upsilon}{d\kappa^2}$ of dispersion function $\upsilon(\kappa)$. Geometry of a dispersion hyperbola $\upsilon = \upsilon_A \cosh\rho$ is such that its bottom ($\rho = 0 = u$) radius of curvature RoC equals the rest frequency $\upsilon_A = M_{rest}c^2/h$ that is labeled as the *b-circle* radius B in Fig. 15. Hyperbola curvature decreases as ρ increases, and so its RoC and M_{eff} grow according to (30) and (31) in proportion to exponential $e^{3\rho}$ as velocity u approaches c, or the *cube* of e^{ρ} for high-ρ growth of momentum mass M_{mom} in (30).

2. *How light is light?*

Since 1-CW dispersion $\upsilon = \pm c\boldsymbol{\kappa}$ is flat, its RoC and photon effective mass are infinite $M^{\gamma}_{eff} = \infty$. This is consistent with the Evenson's axiom prohibiting c-acceleration (*All* colors *always* go c.) . The other extreme is photon rest mass which is zero $M^{\gamma}_{rest} = 0$. Between these extremes, photon momentum-mass M^{γ}_{mom} depends on quality, that is, CW color or frequency υ.

$$\begin{aligned} &(a)\,\gamma{-}\text{restmass}: M^{\gamma}_{rest} = 0, \\ &(b)\,\gamma{-}\text{momentum mass}: M^{\gamma}_{mom} = \tfrac{p}{c} = \tfrac{h\kappa}{c} = \tfrac{h\upsilon}{c^2}, \\ &(c)\,\gamma{-}\text{effective mass}: M^{\gamma}_{eff} = \infty. \end{aligned} \tag{35}$$

Newton's *Optics* text is famous for his rejection of wave nature of light in favor of a corpuscular one. He described interference effects as light's 'fits'. Perhaps, light having three mass values in (35) would, for Newton, verify its schizophrenic insanity. Also, the fact that 2-CW 600THz cavity momentum $\boldsymbol{p}$ must average to zero while each photon adds a tiny mass M^{γ}_{mom}, might support his corpuscular view.

$$M^{\gamma}_{mom} = \frac{h\upsilon}{c^2} = \upsilon(7.4\cdot 10^{-51})kg\cdot s = 4.4\cdot 10^{-36}kg \quad (\text{for }:\upsilon{=}\,600\text{THz}) \tag{36a}$$

A 1-CW state has zero M^{γ}_{rest}, but (*N=1*)-photon momentum (50) is non-zero $p^{\gamma}{=}M^{\gamma}_{mom}c$.

$$p^{\gamma} = h\kappa = \frac{h\upsilon}{c} = \upsilon(2.2\cdot 10^{-42})kg\cdot m = 1.3\cdot 10^{-27}kg\cdot m\cdot s^{-1} \quad (\text{for }:\upsilon{=}\,600\text{THz}) \tag{36b}$$

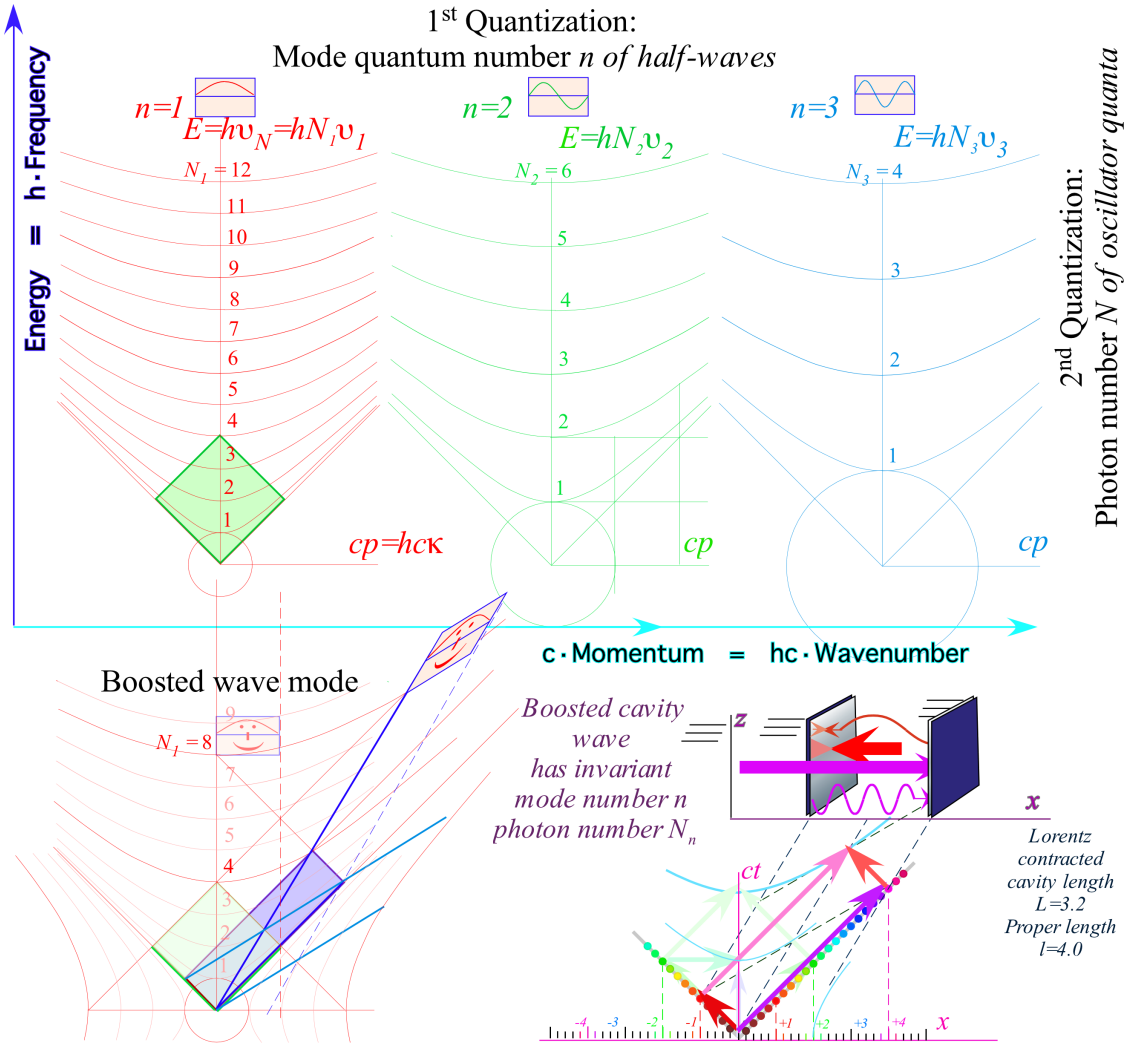

FIG. 16: 1^{st} quantized mode stacks n=1,2,3 of 2^{nd} quantized photon levels N_n=1,2,3..∞

In the form $p^\gamma = M^\gamma_{mom}c$ Galileo's p=MV is exact for light. With numbers so tiny it is a wonder that subtle of a relativistic or quantum effects were ever noticed. Photons are *light*! That is unless the photon quantum number N is huge as in thermonuclear blast[8] (pg.70) or a star[8] (pg.92). Then light can be many tons!

B. Visualizing quantization of Maxwell light waves

Relativity and quantum theory, two pillars of modern (20^{th}-century) physics, are stunning chapters in the long and still evolving story about light. Just forty years before, Maxwell had developed the classical theory of light waves, a stunning alternative to Newton's cor-

puscular theory. Then Planck's 1900 hypothesis of discrete light quanta and Eintein's 1905 photoelectric theory showed light could exhibit both particle and wavelike behavior.

·Since then modern physics has revealed that the *classical* mechanical world has a well hidden underlying wave-like *quantum* mechanical world. There classical quantities such as energy and momentum become "quantized" or restricted to discrete values like notes of a musical instrument. This results in the discrete frequency spectra of atomic matter.

·Quantization occurs when waves resonate in a trap or some kind of cavity or enclosure where they must self-interfere. There results a natural selection by survival-by-the-fittest waves able to fit discrete wave-numbers n of undulations into the enclosure.

1. 1st and 2nd quantization

For light (electromagnetic wave mode sums $\sum A_{\mathbf{k},\omega} e^{i(\mathbf{k}\bullet\mathbf{r}-\omega t)}$) there are two kinds of quantization. 1^{st}-quantization is of phase-($\mathbf{k}\cdot\mathbf{r}$-$\omega t$) variables $\mathbf{k}$ and ω. 2^{nd}-quantization is of field amplitudes $A_{\mathbf{k},\omega}$. Modes for 1^{st}-quantum numbers n=1,2,3,.. of half-waves must fit in a model cavity of length-ℓ and satisfy 1^{st} quantization conditions for ω_n=ck_n in that cavity.

$$wave\,vector:\ k_n=\frac{\pi}{\lambda_n}=n\frac{\pi}{\ell} \qquad \angle-frequency:\ \ \omega_n=ck_n=cn\frac{\pi}{\ell} \tag{37}$$

In Fig.16 a wave-in-cavity is sketched for mode n=1, 2, and 3 above a stack of photon energy levels for 2^{nd}-quantum numbers N_n=1,2,.. of photons. Each photon level-N_n is drawn as a relativistic hyperbola in a stack labeled by mode-n and it photon number. Each hyperbola and its quanta n and N are invariant to transformation of space-time and (ω_n, ck_n).

2^{nd}-quantization of cavity mode k_n (or $\mathbf{k}$ in 3D cavity) uses normal coordinates A_{k_n}=$A_{\mathbf{k}}$ satisfying Maxwell equations reduced to that of harmonic oscillators. A 2-CW-standing-wave vector potential amplitude $A_{\mathbf{k}} \equiv \mathbf{A} = \mathbf{e}_1 |A| \sin(\mathbf{k}\cdot\mathbf{r}-\omega t+\phi)$ has Maxwell $\mathbf{E}$-and-$\mathbf{B}$-fields.

$$\begin{array}{cc} \mathbf{E}=-\dfrac{\partial\mathbf{A}}{\partial t} & \mathbf{B}=\nabla\times\mathbf{A} \\ \mathbf{E}=\mathbf{e}_1 E_0 \cos\ (\mathbf{k}\cdot\mathbf{r}-\omega t+\phi) & \mathbf{B}=(\mathbf{k}\times\mathbf{e}_1)\, B_0 \cos\ (\mathbf{k}\cdot\mathbf{r}-\omega t+\phi) \end{array} \tag{38}$$

Two unit polarization directions $\mathbf{e}_1$ of $\mathbf{E}$ and $\mathbf{e}_2$=$\mathbf{k}\times\mathbf{e}_1\,\frac{1}{k}$ of $\mathbf{B}$ share equal energy.(Let:k=$\frac{\omega}{c}$)

$$(a)\ E_0\mathbf{e}_1=|A|\,\omega\,\mathbf{e}_1 \qquad (b)\ B_0\,(\mathbf{k}\times\mathbf{e}_1)=|A|\ k\mathbf{e}_2 \tag{39}$$

With unit wavevector $\mathbf{e}_k{=}\frac{\mathbf{k}}{k}$ this makes a triad of orthonormal unit vectors $\{\mathbf{e}_1,\mathbf{e}_2,\mathbf{e}_k\}$. Average field energy $\langle U\rangle V$ in a volume V containing the 2-CW vector potential amplitude: $\mathbf{A}{=}\mathbf{e}_1\,|A|\sin(\mathbf{k}{\cdot}\mathbf{r}{-}\omega t{+}\phi)$ is given by Maxwell's relations.

$$\begin{aligned}\langle U\rangle\, V &= \left\langle \frac{\varepsilon_0}{2}\mathbf{E}{\bullet}\mathbf{E}+\frac{1}{2\mu_0}\mathbf{B}{\bullet}\mathbf{B}\right\rangle V = V\left(\frac{\varepsilon_0}{2}|A|^2\omega^2+\frac{|A|^2}{2\mu_0}k^2\right)\left\langle\cos^2(\mathbf{k}\cdot\mathbf{r}-\omega t+\phi)\right\rangle \\ &= \frac{\varepsilon_0}{2}\omega^2|A|^2V=\frac{1}{2\mu_0}k^2|A|^2V \text{ given } (\mathbf{r},\text{t})\text{-average: } \left\langle\cos^2(\mathbf{k}\cdot\mathbf{r}-\omega t+\phi)\right\rangle=\frac{1}{2}\end{aligned} \tag{40}$$

Constants $\epsilon_0{=}8.854{\cdot}10^{-7}\frac{Nm^2}{C^2}$ and $\mu_0{=}4\pi10^{-7}\frac{N}{A^2}$ have geometric mean $c^{-1}{=}\sqrt{\epsilon_0\mu_0}$, a still awe inspiring expression for the speed of light. Feynman's approach to field quantization favors Fourier combinations of complex moving waves $e^{i(kr-\omega t)}$ rather the real forms in (38).

$$\mathbf{A}{=}\sum_{\mathbf{k}}\left[(a_{\mathbf{k}1}\mathbf{e}_1{+}\,a_{\mathbf{k}2}\mathbf{e}_2)\,e^{i(\mathbf{k}\cdot\mathbf{r}-\omega t)}+\text{c.c.}\right]=\sum_{\mathbf{k}}\sum_{\alpha=1}^{2}\left[a_{\mathbf{k}\alpha}\mathbf{e}_\alpha e^{i(\mathbf{k}\cdot\mathbf{r}-\omega t)}{+}a^*_{\mathbf{k}\alpha}\mathbf{e}_\alpha e^{-i(\mathbf{k}\cdot\mathbf{r}-\omega t)}\right] \tag{41}$$

The $\mathbf{k}$-sum $k_\alpha = N_\alpha\frac{2\pi}{\ell}$ $(N_\alpha{=}1,2,\ldots\infty;\ \alpha{=}x,y,z)$ separates 2D polarization base vectors of (39) belonging to its $\mathbf{E}$ and $\mathbf{B}$ oscillator dimensions. Fourier amplitudes $a_{\mathbf{k}\alpha}$ of 1-CW modes in (41) are complex and half the magnitude of the 2-CW amplitude $A_{\mathbf{k}\alpha}$ in (40) since $A\cos\phi{=}\frac{A}{2}(e^{i\phi}{+}e^{-i\phi})$. $\langle U\rangle V$ in (40) and Planck's $\varepsilon_N{=}\hbar N\omega$ relates amplitude A to quanta N.

$$\langle U\rangle V{=}\,\hbar N\omega=\frac{\varepsilon_0}{2}\omega^2|A|^2V \quad\Rightarrow\quad |A|{=}\sqrt{\frac{2\hbar N}{\varepsilon_0\omega V}} \quad\Rightarrow\quad |\mathbf{E}|{=}\,\omega|A|{=}\sqrt{\frac{2\hbar N\omega}{\varepsilon_0 V}} \tag{42}$$

State $|N_{\mathbf{k}\alpha}\rangle$ confined to one quantum level $N_{\mathbf{k}\alpha}$ of one cavity mode $\mathbf{k}$ of one polarization-α is quite different from semi-classical *coherent* laser wave states able to make coordinate grids in Fig.1b and Fig.4b. Laser waves are coherent combinations of harmonic oscillator number states $\{|N_{\mathbf{k}_\alpha}\rangle\}{=}\{..|0_{\mathbf{k}_\alpha}\rangle,|1_{\mathbf{k}_\alpha}\rangle,|2_{\mathbf{k}_\alpha}\rangle,..\}$with Poisson-like distribution coefficients. The coefficients can be set to make amplitude-squeezed waves with minimum amplitude uncertainty, or else phase-squeezed wave nodes desired for sharp coordinate grids in Fig. 1b. Pure photon number $N_{\mathbf{k}_\alpha}$-states have maximum uncertainty for both phase and amplitude that smears (x,ct)-grids. Fig.17 sketches low lying $N_{\mathbf{k}_\alpha}$- quantum oscillator waves discussed below.

2. Quantum numbering of photons and modes

Building 1-CW Fourier expansions of fields **E** and **B** to construct their energies $U_E V$ and $U_B V$ from vector potential **A** in (41).

$$\begin{aligned} U_E V &= \sum_{\mathbf{k}\alpha} \frac{\varepsilon_0 V}{2} \left[2|a_{\mathbf{k}\alpha}|^2 \omega^2 - a^*_{-\mathbf{k}\alpha} a^*_{\mathrm{k}\alpha} \omega^2 e^{-2i\omega t} - a_{-\mathbf{k}\alpha} a_{\mathbf{k}\alpha} \omega^2 e^{-2i\omega t} \right] \\ U_B V &= \sum_{\mathbf{k}\alpha} \frac{\varepsilon_0 V}{2} \left[2|a_{\mathbf{k}\alpha}|^2 \omega^2 + a^*_{-\mathbf{k}\alpha} a^*_{\mathbf{k}\alpha} \omega^2 e^{-2i\omega t} + a_{-\mathbf{k}\alpha} a_{\mathbf{k}\alpha} \omega^2 e^{-2i\omega t} \right] \end{aligned} \tag{43}$$

Cancellation of cross-terms simplifies total energy sum.

$$UV = (U_E + U_B)\, V = \sum_{\mathbf{k}\alpha} 2\varepsilon_0 \omega^2 |a_{\mathbf{k}\alpha}|^2 V = \sum_{\mathbf{k}\alpha} 2\varepsilon_0 V \omega^2 a^*_{\mathbf{k}\alpha} a_{\mathbf{k}\alpha} \tag{44}$$

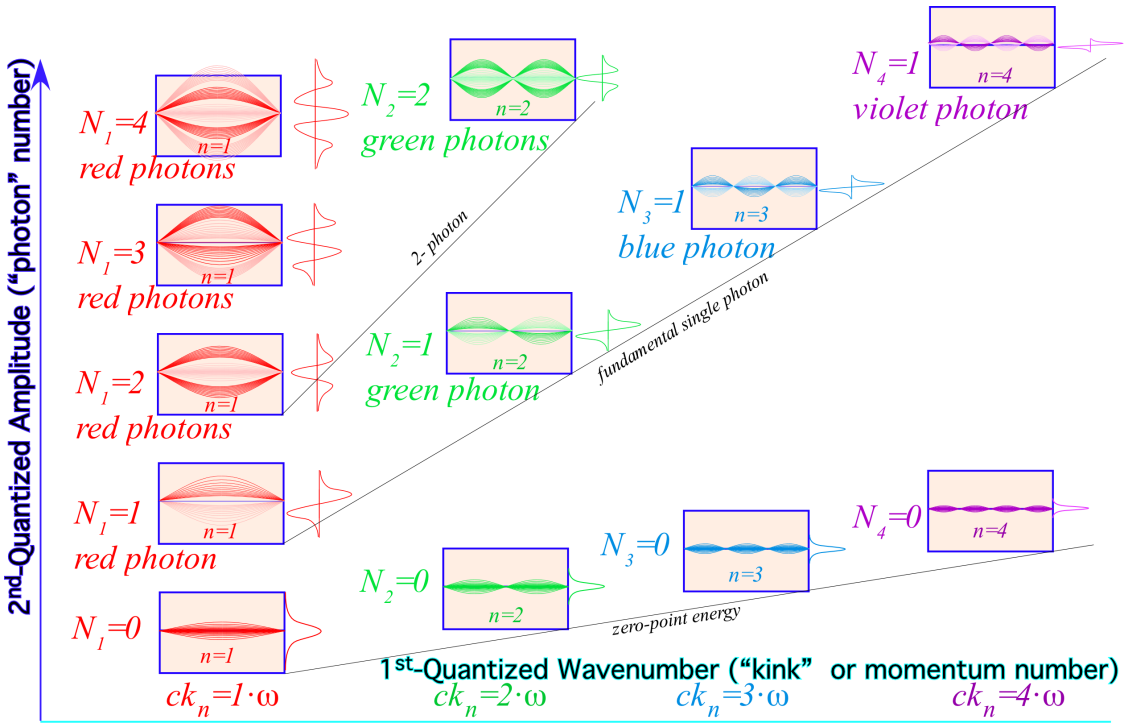

FIG. 17: 1^{st} and 2^{nd} quantized harmonic-oscillator cavity wave sketches.

This may be factored and relabeled into a harmonic oscillator Hamiltonian.

$$\begin{aligned} UV &= \sum_{\mathbf{k}\alpha} \tfrac{1}{2} \left[2\omega\sqrt{\varepsilon_0 V}\left(a^{\mathrm{Re}}_{\mathbf{k}\alpha} - i a^{\mathrm{Im}}_{\mathbf{k}\alpha}\right)\right]\left[2\omega\sqrt{\varepsilon_0 V}\left(a^{\mathrm{Re}}_{\mathbf{k}\alpha} - i a^{\mathrm{Im}}_{\mathbf{k}\alpha}\right)\right] \\ &= \sum_{\mathbf{k}\alpha} \tfrac{1}{2}\left[\omega Q_{\mathbf{k}\alpha} + iP_{\mathbf{k}\alpha}\right]\left[\omega Q_{\mathbf{k}\alpha} + iP_{\mathbf{k}\alpha}\right] \\ &= \sum_{\mathbf{k}\alpha} \tfrac{1}{2}\left(P^2_{\mathbf{k}\alpha} + \omega^2 Q^2_{\mathbf{k}\alpha}\right) \end{aligned} \tag{45}$$

Real and imaginary parts of phasor amplitudes $a_{\mathbf{k}\alpha}$ are coordinates $Q_{\mathbf{k}\alpha}$ and momenta $P_{\mathbf{k}\alpha}$.

$$\begin{aligned} Q_{\mathbf{k}\alpha} &= 2\sqrt{\varepsilon_0 V}\, a^{\mathrm{Re}}_{\mathbf{k}\alpha} = \sqrt{\varepsilon_0 V}\left(a_{\mathbf{k}\alpha} + a^*_{\mathbf{k}\alpha}\right) \quad \text{where: } a_{\mathbf{k}\alpha} = a^{\mathrm{Re}}_{\mathbf{k}\alpha} + i a^{\mathrm{Im}}_{\mathbf{k}\alpha} = \frac{1}{2\sqrt{\varepsilon_0 V}}\left(Q_{\mathbf{k}\alpha} + \frac{iP_{\mathbf{k}\alpha}}{\omega}\right) \\ P_{\mathbf{k}\alpha} &= 2\omega\sqrt{\varepsilon_0 V}\, a^{\mathrm{Im}}_{\mathbf{k}\alpha} = \omega\sqrt{\varepsilon_0 V}\left(a_{\mathbf{k}\alpha} - a^*_{\mathbf{k}\alpha}\right)/i \text{ and: } a^*_{\mathbf{k}\alpha} = a^{\mathrm{Re}}_{\mathbf{k}\alpha} - i a^{\mathrm{Im}}_{\mathbf{k}\alpha} = \frac{1}{2\sqrt{\varepsilon_0 V}}\left(Q_{\mathbf{k}\alpha} - \frac{iP_{\mathbf{k}\alpha}}{\omega}\right) \end{aligned} \tag{46}$$

Amplitudes $a_{\mathbf{k}\alpha}$ and $a^*_{\mathbf{k}\alpha}$ become operators of photon destruction $\mathfrak{a}_{\mathbf{k}\alpha}$ and creation $\mathfrak{a}^\dagger_{\mathbf{k}\alpha}$ that find 2D oscillator waves and energy spectrum for each $\mathbf{k}$-mode and each polarization $\alpha{=}x, y$.

$$E_{\mathbf{k}} = \hbar\Omega_{\mathbf{k}} = \hbar(N_{\mathbf{k}} + 1)\omega_{\mathbf{k}} = \hbar(N_{x,\mathbf{k}} + N_{y,\mathbf{k}} + 1)\omega_{\mathbf{k}} \tag{47}$$

The ground quantum state has zero ($N_{\mathbf{k}}{=}0$) photons with zero-point energy $\hbar\omega_{\mathbf{k}}$. (Zero point energy is $\frac{1}{2}\hbar\omega_{\mathbf{k}}$ for each polarization dimension.) There are two energy-degenerate

states having one photon ($N_{\mathbf{k}}$=1) each with energy $E_{\mathbf{k}}$=$\hbar 2\omega_{\mathbf{k}}$, that is, one photon with x-polarization or else one photon with y-polarization. Similarly, there are three states of two photons ($N_{\mathbf{k}}$=2) with energy $E_{\mathbf{k}}$=$\hbar 3\omega_{\mathbf{k}}$, that is, ($N_{x,\mathbf{k}}$,$N_{y,\mathbf{k}}$)=(2,0), (1,1), or (0,2). A general $N_{\mathbf{k}}$-photon energy level $E_{\mathbf{k}}$=$\hbar(N_{\mathbf{k}}+1)\omega_{\mathbf{k}}$ has polarization degeneracy of $N_{\mathbf{k}}$+1.

A sketch of the first few quantum cavity wave states is given in Fig. 17. It is companion to Fig.16 showing a stack of $N_{\mathbf{k}}$-labeled energy-level hyperbolas for each cavity mode k_n=$\mathbf{k}$. The quantum numbers N (Number of photons) and n (number of "kinks" or anti-nodes per cavity dimension ℓ) are invariant to observer rapidity ρ while wave energy (frequency) and momentum (wave number) vary with observer rapidity as $\cosh\rho$ and $\sinh\rho$, respectively.

V. RELAWAVITY GEOMETRY OF HAMILTONIAN AND LAGRANGIAN FUNCTIONS

The 2-CW matter-wave in Fig.1 has a rest frame with origin $x' = 0$ and $k' = 0 = k_{phase}$ where the invariant phase function $\Phi = kx - \omega t = k'x' - \omega' t'$ reduces to $\Phi = 0 - \varpi\tau$, a product of its proper or base frequency $B = \varpi = Mc^2/\hbar$ defined after (28) with proper time t′=τ defined by (13). The *(x,t)*-differential of phase is reduced as well to a similar negative mass-frequency (ϖ)-term.

$$d\Phi = kdx - \omega dt = 0 \cdot 0 - \tfrac{Mc^2}{\hbar} d\tau \equiv -\varpi d\tau \tag{48}$$

A proper-time interval dτ dilates to ρ-moving frame interval dt by Einstein dilation relations.

$$dt = \frac{d\tau}{\sqrt{1 - u^2/c^2}} = d\tau \cosh\rho \quad \Leftrightarrow \quad d\tau = dt\sqrt{1 - u^2/c^2} = dt\,\mathrm{sech}\rho \tag{49}$$

One of the more interesting tales of modern physics is a first meeting[9] between Dirac[10] and the younger Richard Feynman[11]. Both had been working on aspects of quantum phase and classical Lagrangian mechanics. Dirac mused about some formulas in one of his papers that showed similarities between a Lagrangian function and quantum phase. Feynman said abruptly, "That's because the Lagrangian *is* quantum phase!" That was a fairly radical bit of insight at the time, but it needs its geometry clarified.

A. Phase, action, and Lagrangian functions

Feynman's observation needs some adjustment for units since Lagrangian L has *Joule* units of energy while phase $\Phi{=}kx{-}\omega t$ is a dimensionless invariant. A quantity S called Action is quantum phase Φ scaled by Planck's angular constant $\hbar = \frac{h}{2\pi} = 1.05 \cdot 10^{-34} J \cdot s$ and is the following time integral of L.

$$S \equiv \hbar\Phi \equiv \int L dt \quad \text{where}: \quad \hbar \equiv \frac{h}{2\pi} = 1.05 \cdot 10^{-34} Joule \cdot Second \tag{50}$$

Differentials of action and phase (48) with proper time (49) combine to re-express Ldt.

$$dS \equiv Ldt = \hbar\, d\Phi = -Mc^2 d\tau = -Mc^2\sqrt{1 - u^2/c^2}\ \cdot dt = -Mc^2 dt\, \mathrm{sech}\rho \tag{51}$$

From ρ-frame time derivative $dt/d\tau$ (57) arises the Lagrangian in terms of rapidity ρ or stellar angle σ.

$$L = -Mc^2\sqrt{1 - u^2/c^2} = -Mc^2 \mathrm{sech}\rho = -Mc^2 \cos\sigma \tag{52}$$

Table I supplies identity $\mathrm{sech}\rho = \cos\sigma$ for L in (51) and $\tanh\rho = \sin\sigma$ for group velocity u.

$$u \equiv V_{group} = c\tanh\rho = c\sin\sigma \tag{53}$$

Lagrangian L is conventionally a function of velocity. This is consistent with the low-ρ approximation to Lagrangian (51) that recovers the Newtonian $KE = \frac{1}{2}Mu^2$ term in (27).

$$L = -Mc^2\sqrt{1 - u^2/c^2} \underset{u \ll c}{\longrightarrow} -Mc^2 + \tfrac{1}{2}Mu^2 + ... \tag{54}$$

The explicit functionality for Hamiltonian *H(p)* and Lagrangian *L(u)* involves geometry of Legendre contact transformation shown in Fig.18a-b below and a Fig.19 that follows.

B. Hamiltonian functions and Legendre transformation

The invariant phase differential (48) with scale-factor as in (50) is a key relation.

$$dS \equiv Ldt \equiv \hbar\, d\Phi = \hbar k\, dx - \hbar\omega\, dt \tag{55}$$

Energy $E{=}h\upsilon_{phase}{=}\hbar\omega{=}H$ and momentum $p{=}h\kappa_{phase}{=}\hbar k$ from (28) for $N{=}1$ are used.

$$dS \equiv Ldt \equiv \hbar\, d\Phi = p\, dx - H dt \quad \Rightarrow \quad L = p\frac{dx}{dt} - H = p\dot{x} - H \tag{56}$$

Energy E equals Hamiltonian function H. This gives *Poincare differential invariant* $Ldt{=}pdx{-}Hdt$ and the *Legendre transform* $L{=}pu{-}H$ of Lagrangian L to and from Hamiltonian H. Remarkably, this shows L/Mc^2 is the negative reciprocal of H/Mc^2.

$$H = \hbar\omega \ = Mc^2 \cosh\rho = Mc^2 \sec\sigma = \frac{Mc^2}{\sqrt{1 - u^2/c^2}} \tag{57a}$$

$$L = \hbar\dot{\Phi} = -Mc^2 \mathrm{sech}\rho = -Mc^2 \cos\sigma = -Mc^2\sqrt{1 - u^2/c^2} \tag{57b}$$

Except for a (-)sign, H and L are co-inverse (cos,sec)-functions (middle-columns of Table I). So are Einstein t-dilation and Lorentz x-contraction (10a) and (10b). H is explicit function

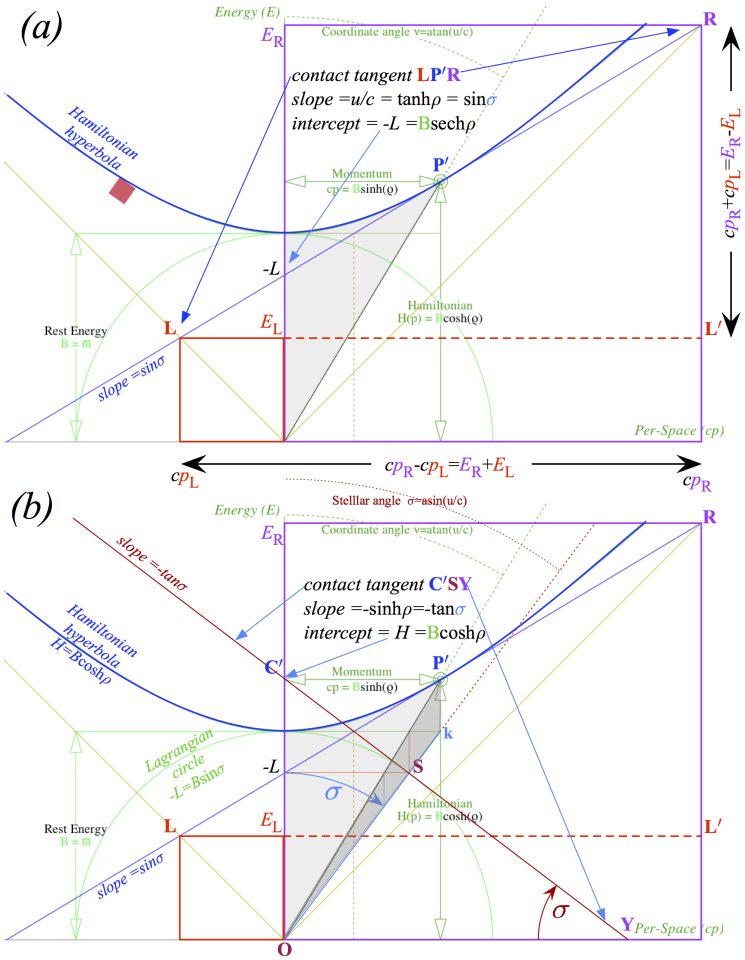

FIG. 18: Legendre transform:

(a) Slope u/c and intercept -L of $H(p)$-tangent $L\mathbf{P}'$ give (u,L) point $\mathbf{S}$ on $L(u)$-circle.

(b) Slope cp and intercept H of $L(u)$-tangent $\mathbf{C}'\mathbf{S}$ give (p,H) point $\mathbf{P}'$ on $H(p)$-hyperbola.

of momentum p. L is explicit function of velocity u. u and p *are* a (sin,tan) pair in Table I.

$$cp = \hbar ck = Mc^2 \sinh\rho = Mc^2 \tan\sigma = \frac{Mcu}{\sqrt{1-u^2/c^2}} \tag{58a}$$

$$u \equiv V_{group} = c\tanh\rho = c\sin\sigma \tag{58b}$$

Legendre contact transformation $H(cp)=pu-L=cpu/c-L$ uses slope u/c and intercept-L of tangent line **LR** contacting H-hyperbola in Fig.18a to locate contact point $L(u)$ of Lagrangian plot. Inverse Legendre contact transformation $L(u)=pu-H$ uses slope p and intercept H of stellar tangent line **C′SY** contacting the L-circle in Fig.18b to locate point $H(p)$ of Hamiltonian plot. This construction is further clarified by separate plots of $H(p)$ in Fig. 19a and $L(u)$ in Fig.19b.

Tangent contact transformation is a concept based upon wave properties and goes back to the Huygens and Hamilton principles discussed below. The basics of this lie in construction of space-time (x,ct) wave-grids given frequency-**k**-vectors $(\upsilon,c\kappa)$ like **P′** and **G′** in Fig. 5. Each **P′** or **G′** coordinate pair $(\upsilon,c\kappa)$ determines lines with speed υ/κ and t-intercept spacing $\tau = 1/\upsilon$ on ct-axis while x-intercept spacing is $\lambda = 1/\kappa$ on x-axis. These phase and group grid lines make Minkowski zero-line coordinates.

This geometry applies as well to energy-momentum $(E,cp)=h(\upsilon,c\kappa)=\hbar(\omega,ck)$ spaces. Functional dependence of wave grid spacing and slopes determines classical variables, equations of motion, as well as functional non-dependence. For example, Lagrangian L is an explicit function of velocity u but not momentum p, that is, $\frac{\partial L}{\partial p} = 0$. Hamiltonian H is explicit function of momentum p but *not* velocity u, that is, $\frac{\partial H}{\partial u} = 0$. Such 0^{th}-equations combined with $L=pu-H$ give 1^{st}-Hamilton and 1^{st}-Lagrange equations.

$$0 = \frac{\partial L}{\partial p} = \frac{\partial}{\partial p}(pu-H) \Rightarrow u = \frac{\partial H}{\partial p} \left(\begin{smallmatrix} Hamilton's \\ 1^{st} equation \end{smallmatrix}\right) \tag{59a}$$

$$0 = \frac{\partial H}{\partial u} = \frac{\partial}{\partial u}(pu-L) \Rightarrow p = \frac{\partial L}{\partial u} \left(\begin{smallmatrix} Lagrange \\ 1^{st} equation \end{smallmatrix}\right) \tag{59b}$$

In Fig.18a slope of $H(p)$-hyperbola at tangent contact point **P′** is group velocity $u/c=\tanh\rho=\sin\sigma=3/5$. In Fig.18b slope of $L(u)$-circle at tangent point **S** is momentum $cp=B\sinh\rho=B\tan\sigma=(Mc^2)\frac{3}{4}$ with a minus (-) sign. This minus sign in (57b) for Lagrangian $L=-Mc^2\cos\sigma$, for example, is a result of (-) in basic phase $(kx-\omega t)$ and phasor conventions. (It makes phasor clocks turn clockwise.($\curvearrowright$)) For a low-($\rho \approx u/c$) approximate Lagrangian (54), one may drop the $-Mc^2$ term and just keep the Newtonian kinetic energy term ($\frac{Mu^2}{2}$) that is equal to the

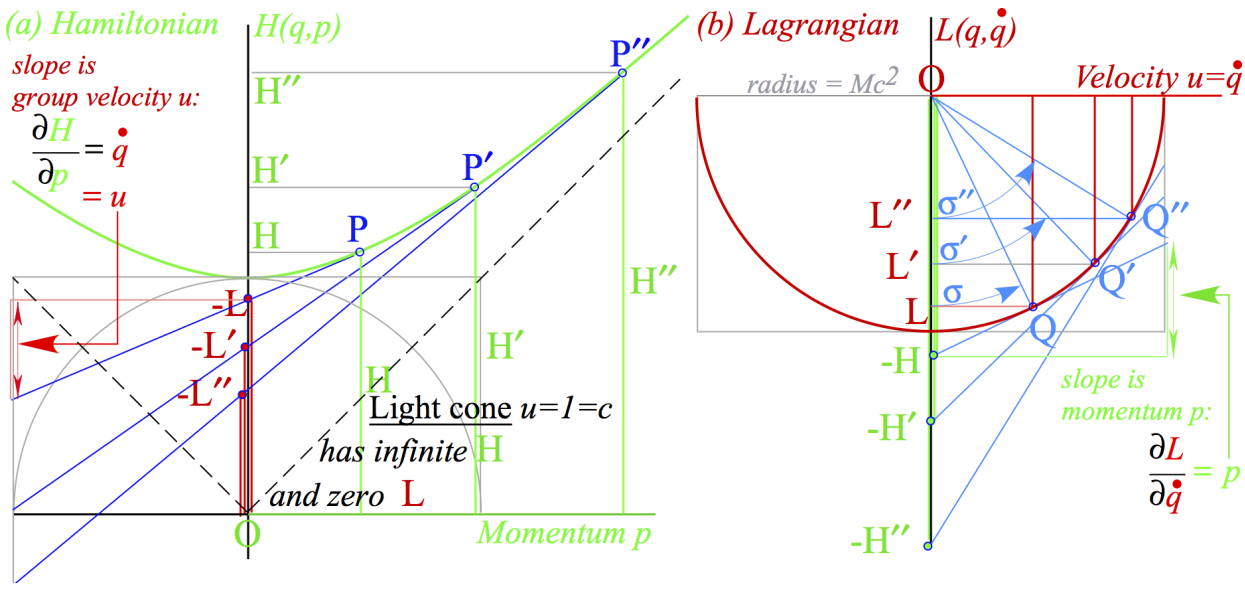

FIG. 19: Relativistic Legendre contact transformation between (a)Hamiltonian $H(p)$ (b) Lagrangian $L(u)$.

corresponding kinetic term ($\frac{p^2}{2M}$) in the approximate Hamiltonian. Of course, that reduces to $\frac{Mu^2}{2}$ if approximate momentum p=Mu is used, so students are well to ask, "Why be so fussy to have only momentum p-dependence of H and only velocity u-dependence of L?"

It is true that Hamiltonian $H(p)$ hyperbola minimum in Fig.18 or Fig.19a is nearly identical to the Lagrangian $L(u)$ circle minimum in Fig.18b that lies below Fig.19b. There both curves are nearly parabolic. But, at higher speeds the Lagrangian $L(u)$ circle approaches zero precipitously as stellar angle σ approaches $\pi/2$ and velocity u approaches c. Meanwhile, the hyperbolic Hamiltonian $H(p)$=$B\cosh\rho$ and its momentum p=$B\sinh\rho$ each zoom away to approach $Be^{\rho/2}$ as rapidity ρ grows without bound. So it should be clear that hyperbolic "country-cousin" functions involving rapidity ρ and momentum p must share a Hamiltonian with infinite horizon, while circular "city-cousin" functions of the very restricted stellar angle $-\pi \leqslant \sigma \leqslant \pi$ and velocity $-c \leqslant u \leqslant c$ must share a localized Lagrangian that is the keeper of quantum phase. The third (csc,cot)-cousin pair phase=$B\operatorname{csch}\rho$=$B\cot\sigma$ and V_{phase}=$B\coth\rho$=$B\csc\sigma$ from Table I do not appear in any discussions of classical correspondence. Instead, these describe the phase part or "quantum guts" of a 2-CW internal structure, and as such were nonexistent for 19-century classicists, and one might add, still today a bit sketchy and hard to observe. Now phase is seen as the "heartbeat" of quantum

physics one may note DeBroglie wavelength phase and velocity V_{phase} in Fig.20 at the lower edges of geometric constructions just inside the Doppler blue shift (b=eρ)-bottom line of the **R** box. One may compare Fig.20 to Trigonometry Road Map (TRM) in Fig.8. They share points **P**=$\frac{1}{2}$(**R**+**L**) and **G**=$\frac{1}{2}$(**R**-**L**). Fig.8 exhibits fundamental and ancient geometry with triangular relations that have fundamental roles in Fig. 20 to describe a relawavity of relativistic quantum mechanics.

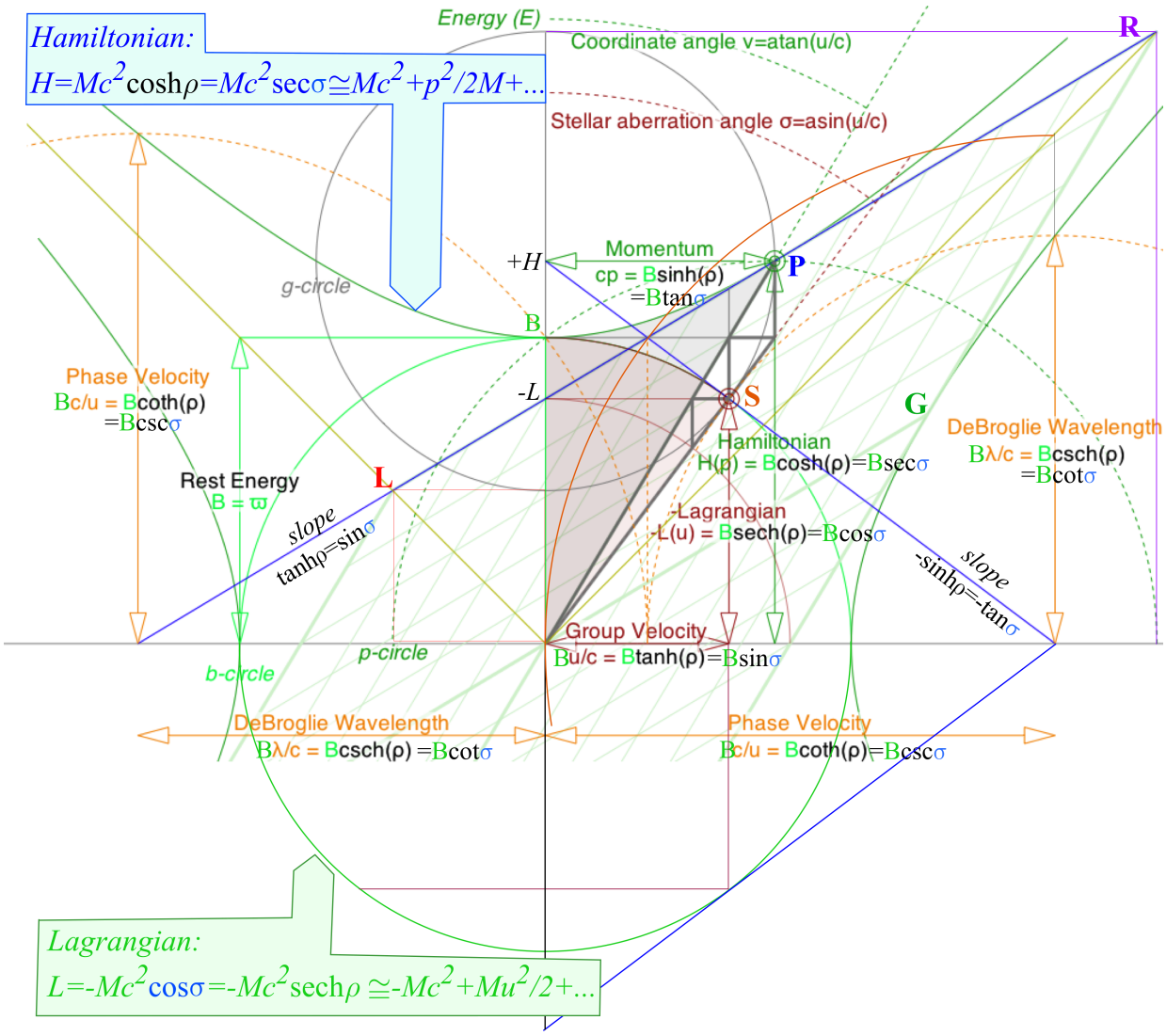

FIG. 20: Geometric elements elements of Hamiltonian and Lagrangian relativistic quantum mechanics.

C. Hamilton-Jacobi quantization

Invariant phase Φ or action S differential (64)-(65) are integrable under certain conditions.

$$dS \equiv Ldt \equiv \hbar\, d\Phi = pdx - Hdt = \hbar k dx - \hbar\omega dt \tag{60}$$

Each coefficient of a differential term dq in dS must be a corresponding partial derivative.

$$\frac{\partial S}{\partial x} = p, \qquad\qquad \frac{\partial S}{\partial t} = -H. \tag{61}$$

These are known as *Hamilton-Jacobi* equations for the phase action function S. Classical HJ-action theory serves to analyze families of trajectories (PW or particle paths). Dirac and Feynman related this to matter-wave mechanics (CW phase paths) by proposing approximate semi-classical wavefunction Ψ based on Lagrangian action $S{=}\hbar\Phi$ in its phase.

$$\Psi \approx e^{i\Phi} = e^{iS/\hbar} = e^{i\int L\, dt/\hbar} \tag{62}$$

Approximation symbol ($\approx$) indicates that phase but not amplitude is expected to vary here. HJ-form $\frac{\partial S}{\partial x} = p$ turns x-derivative of Ψ into standard quantum $\mathbf{p}$-operator form $\mathbf{p} = \frac{\hbar}{i}\frac{\partial}{\partial x}$.

$$\frac{\partial}{\partial x}\Psi \approx \frac{i}{\hbar}\frac{\partial S}{\partial x}e^{iS/\hbar} = \frac{i}{\hbar}p\Psi \qquad \Rightarrow \qquad \frac{\hbar}{i}\frac{\partial}{\partial x}\Psi = \mathbf{p}\Psi \tag{63a}$$

HJ-form $\frac{\partial S}{\partial t} = -H$ turns t-derivative of Ψ similarly into Hamiltonian operator $\mathbf{H} = \hbar i\frac{\partial}{\partial t}$.

$$\frac{\partial}{\partial t}\Psi \approx \frac{i}{\hbar}\frac{\partial S}{\partial t}e^{iS/\hbar} = -\frac{i}{\hbar}H\Psi \qquad \Rightarrow \qquad i\hbar\frac{\partial}{\partial t}\Psi = \mathbf{H}\Psi \tag{63b}$$

Action integral $S = \int Ldt$ is to be minimized. Feynman's interpretation of this is depicted in Fig.21. Any mass M appears to fly so that its phase proper time τ is maximized. The proper mass-energy frequency $\varpi = Mc^2/\hbar$ is constant for a mass M. Minimizing -$\varpi\tau$ is thus the same as maximizing +τ. Clocks near light cone tick slowly compared ones near max-τ. Those on light cone do not tick at all!

One may explain how a flying mass finds and follows its max-τ path by imagining it is first a wave that could spread Huygen's wavelets out over many paths. But, an interference of Huygen wavelets favors stationary and extreme phase. This quickly builds constructive interference in the stationary phase regions where the fastest possible clock path lies. Nearby paths contain a continuum of non-extreme or non-stationary wavelet phase that interfere destructively to crush wave amplitude off the well-beaten max-τ path as seen in Fig. 22.

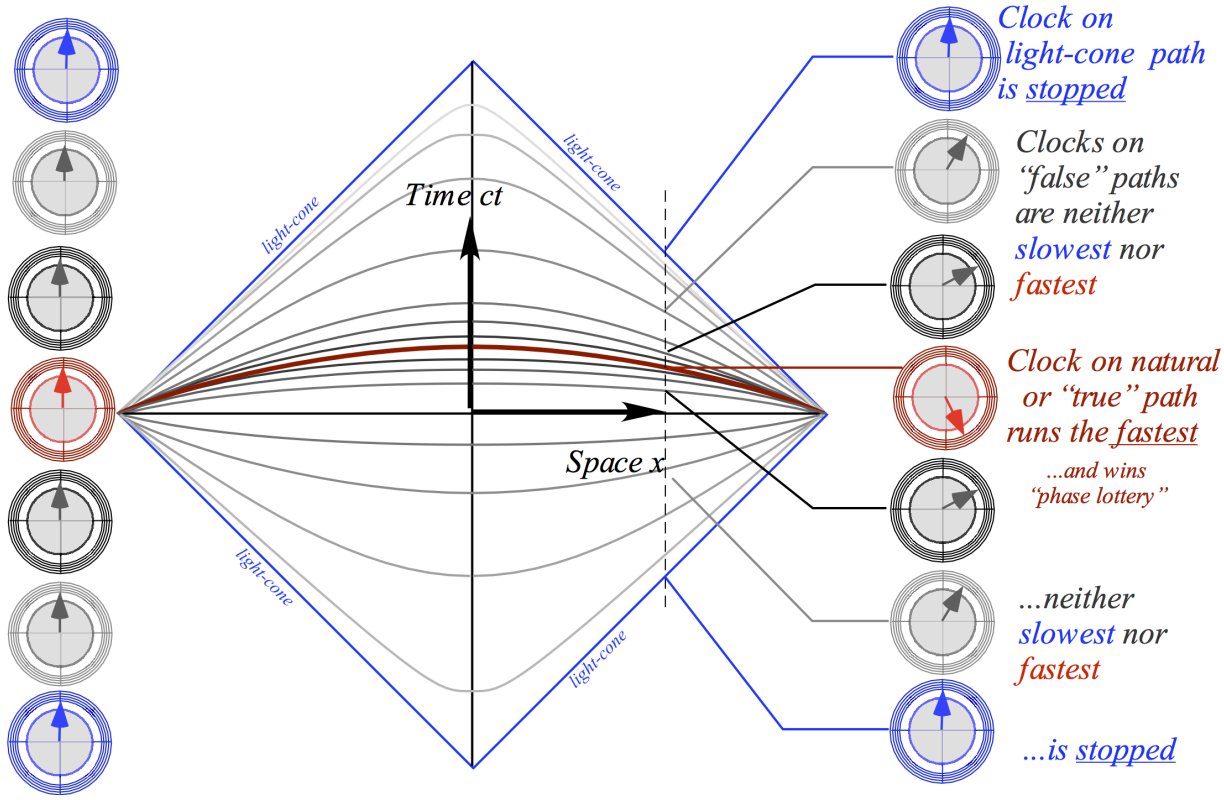

FIG. 21: Feynman's flying clock contest where winner has the greatest advance of time.

The very "best" are so-called *stationary-phase* rays that are extremes in phase and thereby satisfy Hamilton's Least-Action Principle requiring that $S = \int Ldt$ is minimum for "true" classical trajectories. This in turn enforces Poincare invariance by eliminating, by de-phasing, any "false" or non-classical paths because they do not have an invariant (and thereby stationary) phase. So "bad" rays cancel each other in a cacophonous mish-mash of mismatched phases.

Each Huygen wavelet in Fig. 22 is tangent to the next wavefront being produced. That contact point is precisely on a ray or true classical trajectory path of minimum action and on the resulting "best" wavefront. Time evolution from any wavefront to the next is thus a contact transformation between two wavefronts described by geometry of Huygens Principle.

Thus a Newtonian clockwork-world appears to be the perennial cosmic gambling-house winner in a kind of wave dynamical lottery on an underlying wave fabric. Einstein's God may not play dice[12], but some persistently wavelike entities seem to be gaming at enormous $Mc^2/\hbar$-rates down in the cellar! And in so doing, geometric order is somehow created out of

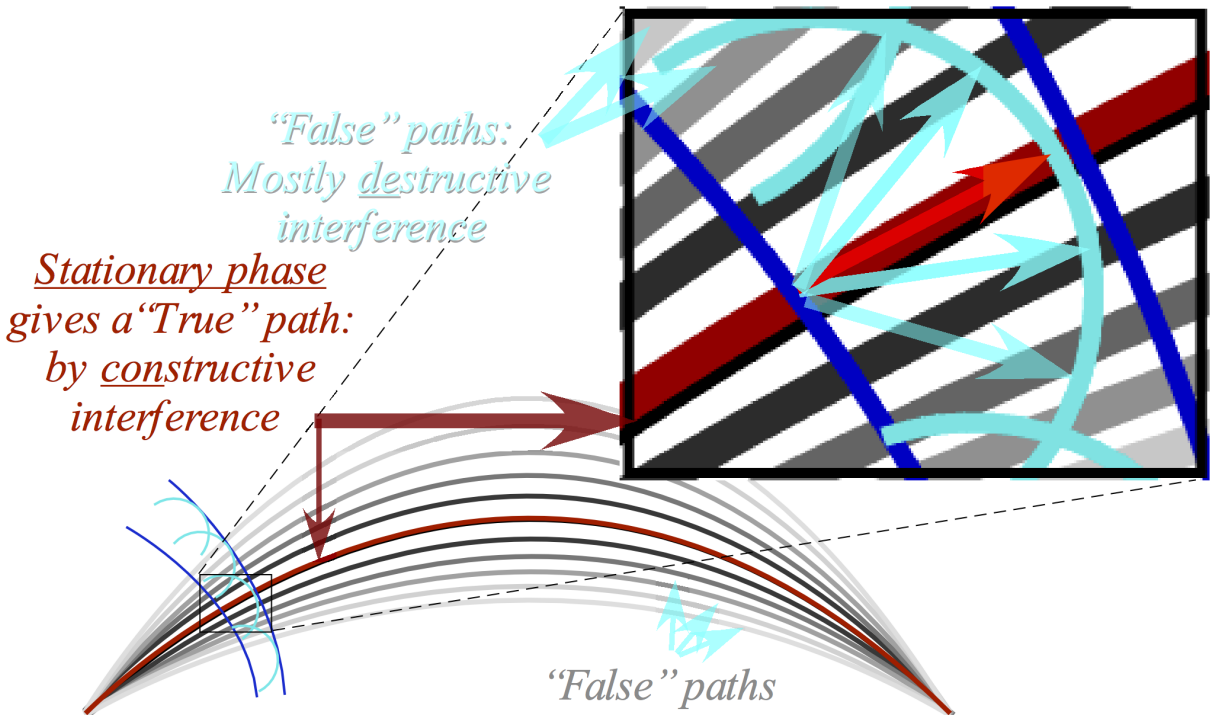

FIG. 22: Quantum waves interfere constructively on "True" path but mostly cancel elsewhere.

what seems like chaos.

It is ironic that Evenson and other metrologists have made the greatest advances of precision in human history, not with metal bars or ironclad classical mechanics, but by using the most ethereal and dicey stuff in the universe: *light waves*. This motivates a view of classical matter or particle mechanics that is more simply and elegantly done by its relation to light and its built-in relativity, resonance, and quantization that occurs when waves are subject to boundary conditions or otherwise confined. While Newton was grousing about "fits" of light, perhaps his crazy stuff was just trying to tell him something!

Derivation of quantum phenomena using a classical particle paradigm seems as silly now as deriving Newtonian results from an Aristotelian paradigm. It now seems much more likely that particles are made by waves, optical or otherwise, rather than vice versa as Newton believed. Also, CW trumps PW as CW axioms of Evenson (*All colors go c.*) and Doppler time-reversal (r=$1/b$) can easily derive Lorentz-Einstein-Minkowski algebra and geometry summarized in Table I and re-derive exact relations (28) for relativity and quantum wave mechanics using geometry summarized in Fig. 20. It all reduces to a redrawn trigonometry

lesson based on Fig.7 and Fig.8.

VI. RELATIVISTIC OPTICAL TRANSITIONS

This elementary development of SR and then QM rests upon the surprising behavior of a pair of ideal laser continuous waves (CW). (A more detailed treatment would show that CW also denotes a Coherent Wave, that is, a coherent state combination of photon-number states of quantum field.) A single continuous wave (1CW) has no rest frame, rest energy, or rest mass.

However, a suitably arranged pair of CW (or 2CW) has non-zero parameters for all three, namely group velocity $u{=}ctanh\rho$ of its rest frame in which 2CW lab energy (Hamiltonian) H=Mc2coshρ is reduced to a minimum value Mc^2 of rest energy due to its rest mass M at just the point where its 2CW lab momentum p=Mcsinhρ vanishes.

So an elementary model that promised less mysterious pedagogy finally confronts our greatest mystery wherein a box of 2CW light obeys rules of mechanics for massive particles where their mass, energy, and momentum depend upon a total phase frequency υphase and wavenumber phase according to (28). As given after (28) the mass-frequency relation is proportional with constants N, h, and $1/c^2$.

$$M = Nh\upsilon_{phase}/c^2 = N\hbar\omega_{phase}/c^2 (h = 6.626 \cdot 10^{-34} J \cdot s, \hbar = 1.05 \cdot 10^{-34} J \cdot s) \qquad (64)$$

The tiny proportionality constant of Planck ($\hbar \sim 10^{-34}$) and ($1/c^2 \sim 10^{-17}$) means the quantum number N and phase frequency υ_{phase} have to be enormous to make appreciable mass out of 2CW light.

Now this mysterious mass model is extended to describe transitions in which a mass (presumably a molecular, atomic, or nuclear particle) emits or absorbs light quanta or *photons*. The geometric analysis of photon-affiliated transitions begins with the simple Doppler shifted or Lorentz transformed "baseball-diamond" geometry shown in Fig. 23. Most figures showing this geometry so far, including Fig.18, Fig.20 and the original Fig.4, are drawn for velocity $u/c{=}3/5$ or Doppler shift $b{=}2$. Here, Fig.23 uses odd values $b{=}3/2$ or $u/c{=}5/13$ to avoid distracting crossings. The Planck-Einstein-DeBroglie relation (28) is labeled by energy $E{=}\hbar\Omega$ plotted versus c-scaled momentum $cp{=}\hbar ck$ so that both have the same dimensions of energy.

A. Photon transitions obey rocket-science formula

Tiny photon momentum $p{=}\hbar k$ needs a c-factor to show up in plots. Also, Fig.23 is bisected by a wavy right-angle **HP′K** inscribed in a g-circle that represents photon (ω,ck)-vectors connecting levels of high-state at rest frequency $\omega_h{=}3$, middle-state at $\omega_m{=}2$, and low-state at $\omega_\ell{=}4/3$. Each frequency relates to one above it (or below it) by blue-shift factor $\mathrm{e}^{+\rho}$ =3/2 (or red-shift factor $\mathrm{e}^{-\rho}$ =2/3). Thus the middle frequency $\omega_m{=}2$ is the geometric mean of those above and below.

$$3 = \omega_h = e^{+\rho}\omega_m \qquad 2 = \omega_m = e^{+\rho}\omega_\ell \qquad \frac{4}{3} = \omega_\ell = e^{-\rho}\omega_m = e^{-2\rho}\omega_h \tag{65}$$

Wavy segment **HP′** represents a photon of energy $\hbar\Omega_{\mathrm{HP}'} = \hbar\omega_m \sinh\rho$ that would be emitted in a transition from a stationary mass $M_{\mathrm{H}} = \hbar\omega_h/c^2$ at point **H** to a mass $M_{\mathrm{H}} = \hbar\omega_h/c^2$ moving with rapidity ρ at point **P′**. Implicit in Fig.23 is the choice of right-to-left direction for the outgoing photon momentum $cp = -\hbar\omega_m \sinh\rho$ recoiling left-to-right by just enough to conserve momentum. Mass M_H loses energy (frequency) equal to momentum (wavevector) of outgoing photon. Since M_H is initially stationary, it must lose energy by reducing rest-mass from M_H to M_P by Doppler shift ratio $e^{+\rho}$.

$$\frac{M_{\mathrm{H}}}{M_{\mathrm{P}}} = \frac{\omega_h}{\omega_m} = e^{\rho} \tag{66}$$

A rest mass formula results for recoil rapidity ρ with a simple low-ρ ($\rho \approx$u/c)-approximation.

$$\rho = \ln\frac{M_{\mathrm{H}}}{M_{\mathrm{P}}} \xrightarrow[\rho\to\frac{u}{c}]{} u = c\ln\frac{M_{\mathrm{H}}}{M_{\mathrm{P}}} \tag{67}$$

Interestingly, this quantum recoil formula is reminiscent of a famous rocket formula.

$$V_{burnout} = c_{exhaust}\ln\frac{M_{initial}}{M_{final}} \tag{68}$$

Quantum transitions are said to be infinite discrete "jumps"with emitted (or absorbed) photons acting like bullets. This contrasts with a relativistic picture of an atom or nucleus in (66) gradually "exhaling"its mass like a rocket with an optical exhaust velocity of c.

The **H**-to-**P′** transition just discussed could be followed by a **P′**-to-**K** transition with forward emission of a photon with the same energy and further reduction of mass from M'_P to a stationary mass M_K at lowest energy level $\hbar\omega_\ell = M_K c^2$ in Fig.23. It has frequency ω_ℓ = 4/3 and zero momentum due to its leftward recoil from rightward emitted photon.

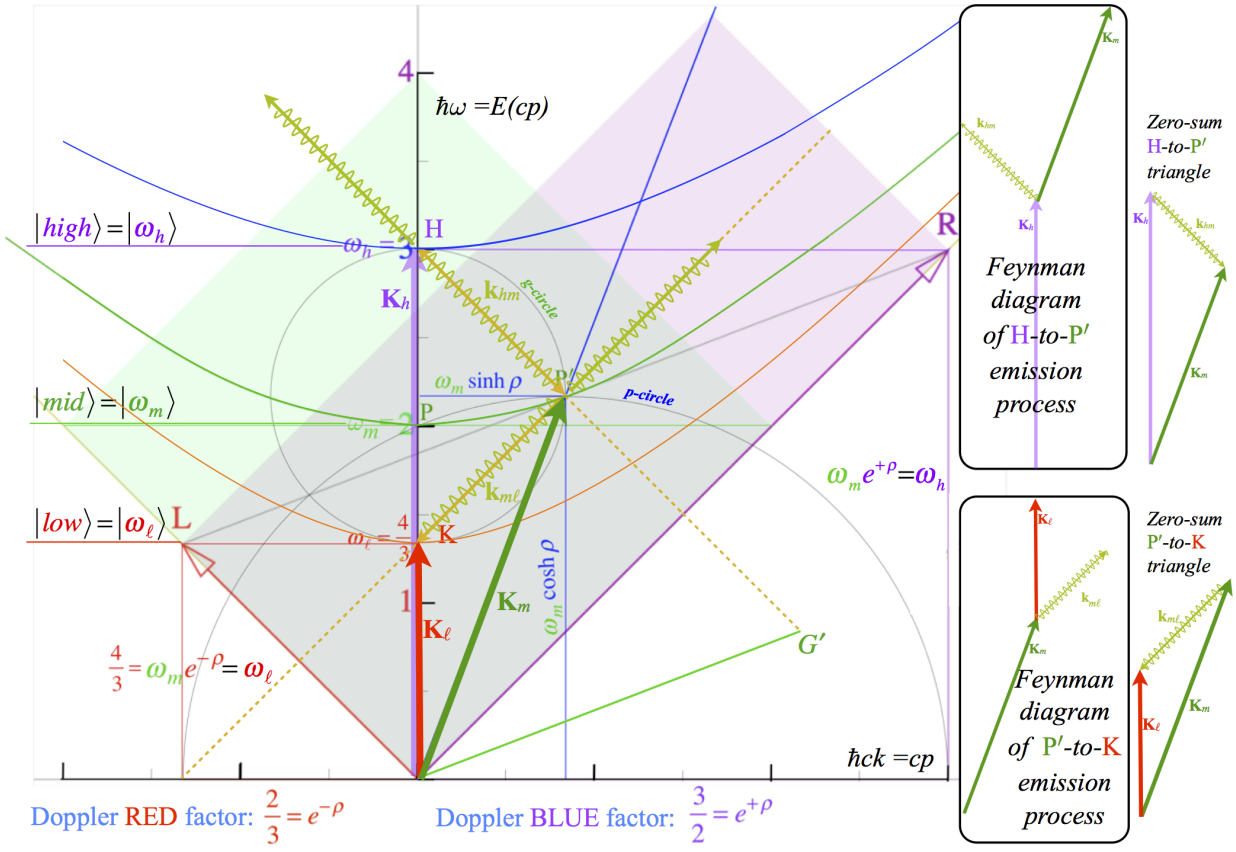

FIG. 23: Feynman diagrams of 1-photon transitions connecting 3-levels ω_h, ω_m, and ω_ℓ.

Feynman diagrams in right-hand inset panels of Fig. 23 are scale models of photon energy-momentum k_{ab}-vectors emitted from head of initial mass-M_A,$\mathbf{K}_A$-vector on the tail point of recoiling mass-M_B,$\mathbf{K}_B$-vector. One may imagine per-space-time (ω,k) diagrams as space-time (x,ct) mass and photon tracks due to Fourier reciprocity demonstrated in Fig. 4 and Fig. 5. Also $\mathbf{K}$-vectors rearrange into head-to-tail zero-sum triangles representing energy-momentum conservation for perfectly resonant transitions.

B. Geometric level and transition sequences

Level sequence $\{\ldots, \omega_\ell, \omega_m, \omega_h, \ldots\}$ in (65) is part of an infinite geometric series having blue-shift ratio $b{=}e^{+\rho}{=}\frac{3}{2}$ or red-shift ratio $r{=}e^{-\rho}{=}\frac{2}{3}$ ranging from 0 to ∞. The energy $E_m = \hbar\omega_m$ or frequency ω_m value labeling hyperbola-ω_m may be scaled to give an infinite

sequence based on ratio $b_1{=}\frac{3}{2}{=}r^{-1}$.

$$\ldots, r^3\omega_m, r^2\omega_m, r^1\omega_m, b^0\omega_m, b^1\omega_m, b^2\omega_m, b^3\omega_m, \ldots, b^q\omega_m, \ldots \tag{69}$$

This labels a geometric sequence stack of hyperbolas shown in Fig.24. Meanwhile, rapidity $\rho = \ln\frac{3}{2}$ labeling velocity line-$(u/c{=}\frac{5}{13})$ is boosted through a sequence of ρ_p-values $\{..., -2\rho\,, -\rho\,, 0\,, 2\rho\,, 3\rho\,, .., p\rho\,, ..\}$ and defines p-points of momentum $cp_{p,\,q}{=}b^q\omega_m\sinh\rho_p$ (where: $\rho_p = \mathrm{p}{\cdot}\rho$) on each $b^q\omega_m$-hyperbola.

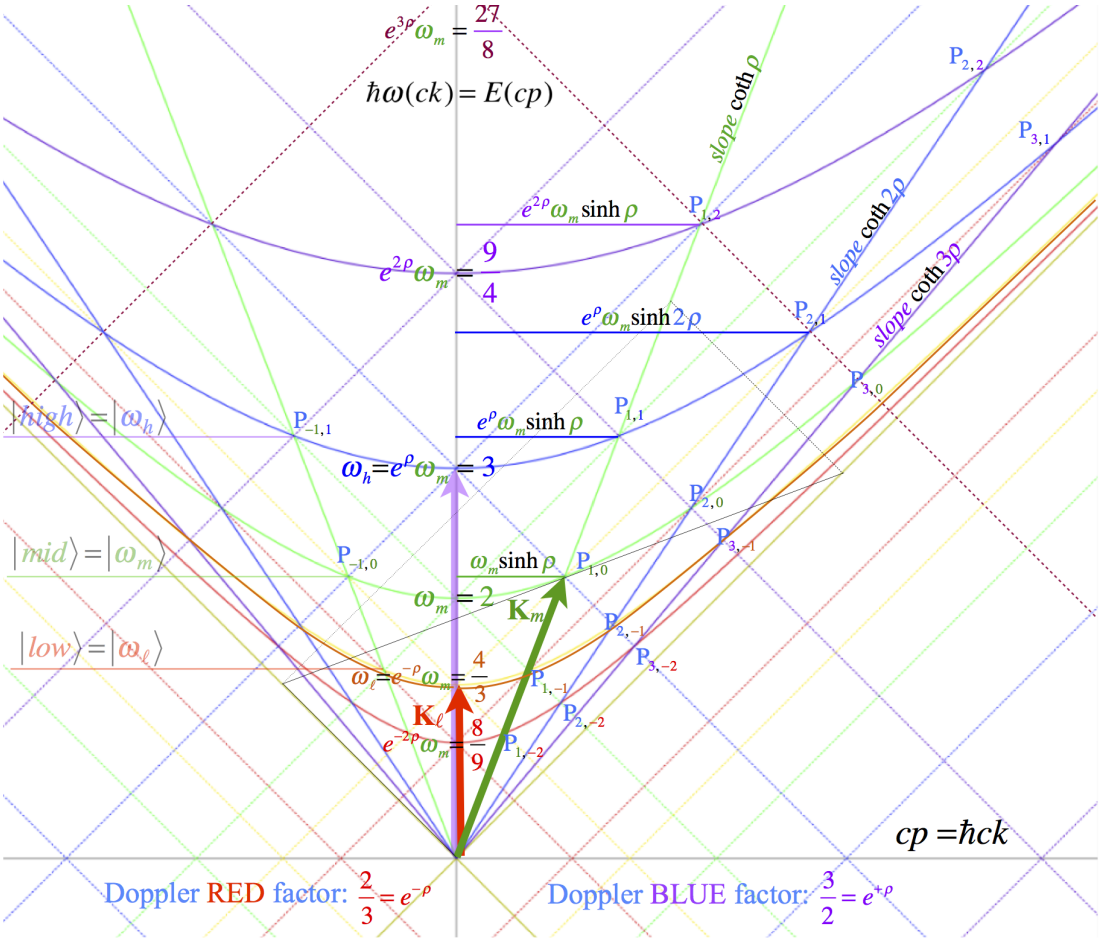

FIG. 24: Rapidity-$\rho_p{=}\mathrm{p}\rho$ and rest-frequency-$\omega_m\mathrm{e}^{q\rho}$ and $\mathrm{P}_{p,q}$-lattice based on integer powers of $b{=}e^{+\rho} = \frac{3}{2}$.

The result is a lattice in Fig.24 of transition points $\mathrm{P}_{p,q}{=}(\mathrm{cp}_{p,q}\ ,\mathrm{E}_q)$ that are scaling-and-Lorentz-boost-equivalent to the point $\mathrm{P}'{=}\mathrm{P}_{1,0}$ at the center of Fig.24 or else the point $\mathrm{P}'{=}\mathrm{P}_{1,0}$ that is the center of transitions in that figure. Choice of origin is quite arbitrary in a symmetry manifold defined by group operations. The $\pm45°$-light-cone boundaries and their

intersection *(cp,E)=(0,0)* lie outside of this open set of $P_{p,q}$ points. The choice of the base Doppler ratio $b=e^{\rho}$ is also arbitrary and may be irrational. However, a rational b guarantees all 16 functions in Table I are also rational. The lattice in Fig. 24 may be viewed at ±45° as a quasi-Cartesian grid of lines. Each line is positioned according to rest-frequency power $\omega_m e^{q\rho}$ at its meeting point on the vertical ω-axis (or 2^{nd}-base of a Doppler baseball diamond) as shown in Fig 21. The +45° R-axis (1^{st}-baseline) is marked-off by sequence $\omega_R=\omega_m e^{R\rho}$ (R=-2,-1,0,1,2...) and the -45° L-axis (3^{rd}-baseline) is marked-off by sequence $\omega_L=\omega_m e^{L\rho}$ (L=-2,-1,0,1,2...). (Here base constants $b=e^{\rho}=\frac{3}{2}$ and $\omega_m=2$ are fixed.) At the intersections of R and L grid-lines are discrete transition (p,q)-points $P_{p,q}$.

$$P_{p,q} = (ck_{p,q}, \omega_{p,q}) = \omega_m e^{q\rho}(\sinh p\rho, \cosh p\rho) \tag{70}$$

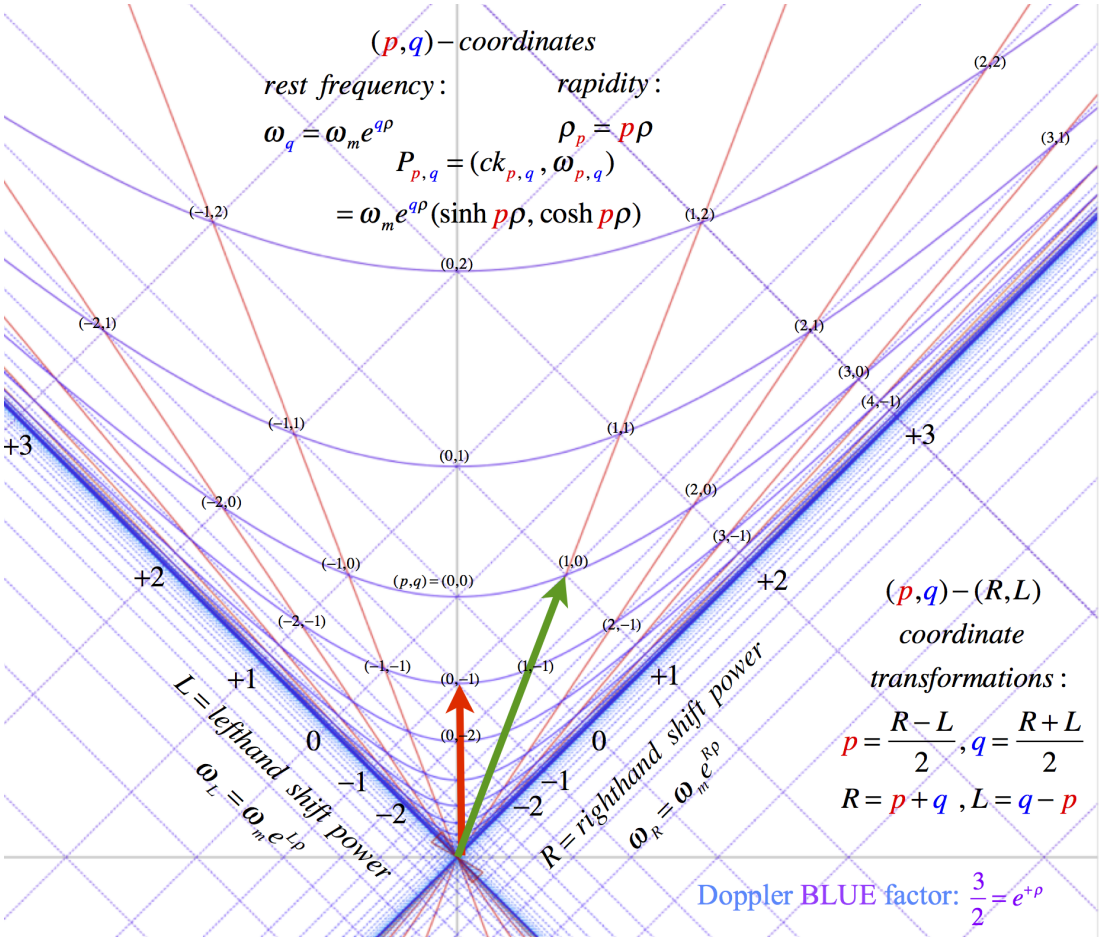

FIG. 25: Hyperbolic lattice of (p,q)-transition points for base b = e^{ρ} = $\frac{3}{2}$ and half-sum-difference coordinate relations.

C. Half-sum-and-difference transition web

Each coordinate point is related by half-sum or half-difference coordinate transformations.

$$p = \frac{R-L}{2}, \;\; q = \frac{R+L}{2} \quad \Leftrightarrow \quad R = p+q, \;\; L = q-p \tag{71}$$

These are integer versions of the phase and group relations (5) and (7) to right and left laser **K**-vectors, yet another result of factoring optical wave coordinate functions. The geometric structure represented here might become a useful basis for a kind of lattice-gauge theory to explore cavity quantum electro-dynamics (CQED) or pseudo-relativistic theories of graphene gauge dynamics.

Such a structure offers a possible solution to the flaw that made Feynman path integration so difficult due its uncountable universe of possible paths. The structure in Fig. 25 offers a labeling of every discrete path and state by an operation in a discrete subgroup of the continuous Poincare-Lorentz group (PLG) that has a discrete Poincare-Lorentz algebra (PLA). The discrete paths may be made as fine as desired so that each PLA becomes a larger and better approximation to the parent PLG. Each PLA has a discrete spectral decomposition that could derive and solve a range of Hamiltonian eigensolutions and transition amplitudes parametrized by discrete paths.

LIST OF FIGURES

LIST OF TABLES